


## Projecting aridity from statistically downscaled and bias-corrected variables for the Gediz Basin, Turkey

Umut Kirdemir <sup>b,c,\*</sup>, Umut Okkan<sup>c</sup> and Okan Fistikoglu<sup>a</sup>

<sup>a</sup> Department of Civil Engineering, Dokuz Eylul University, Izmir, Turkey

<sup>b</sup> The Graduate of School of Natural and Applied Sciences, Hydraulic, Hydrology and Water Resources Division, Dokuz Eylul University, Izmir 35160, Turkey

<sup>c</sup> Department of Civil Engineering, Balikesir University, Balikesir, Turkey

\*Corresponding author. E-mail: umut.kirdemir@gmail.com

 UK, 0000-0001-5336-4842

### ABSTRACT

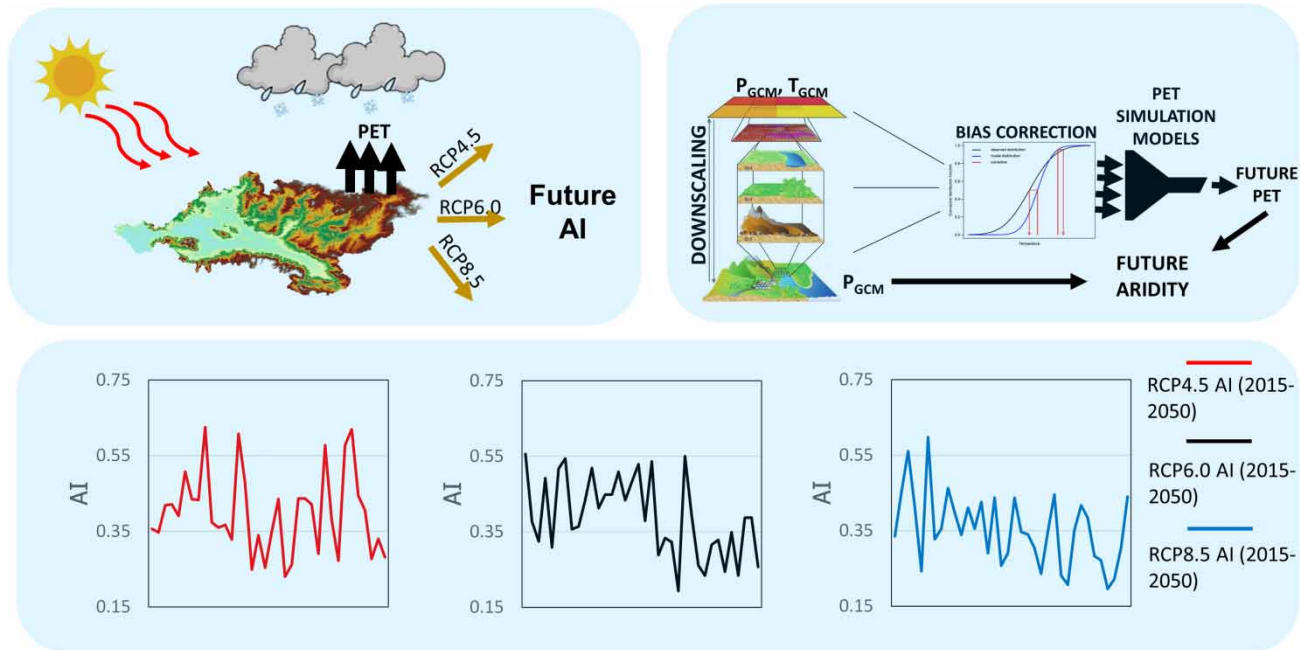
Due to climatological changes, a study was conducted in the Gediz Basin, Turkey, where agricultural production holds an important place. In the study prepared, 12 general circulation models (GCMs) were utilized under representative concentration pathway (RCP)4.5, RCP6.0, and RCP8.5 scenarios of the fifth assessment report (AR5) of IPCC for the period 2015–2050. The statistical downscaling methods were employed and the projections were derived right after applying the weighted-averaged ensemble mean by the Bayesian Model Averaging (BMA) method and bias correction by equidistant quantile mapping (EDQM). The temperature-based potential evapotranspiration (*PET*) formulas were modified in accordance with the Penman–Monteith method and the aridity indexes were calculated by UNEP's formula. According to the projections, the mean annual temperature increases between 1.5 and 2.2 °C and the mean total annual *PET* increases between 5 and 8% are foreseen in the Gediz Basin for the near future. It is foreseen that a semi-arid climate regime may predominate over the region for all of the RCP scenarios under the increasing dryness in basin climate. In addition, it was obtained in the study that sub-humid climate state occurrence for all of the regions included by the basin may be unexpected in the future for the RCP8.5 scenario. The presence of semi-arid climate conditions may be more potent with the increasing trend of radiative forcing over time.

**Key words:** aridity index, Bayesian Model Averaging, equidistant quantile mapping, statistical downscaling

### HIGHLIGHTS

- Artificial intelligence methods were performed for downscaling.
- A multi-model ensemble strategy was carried out for climate projection.
- A robust bias-correction method was utilized.
- Climate change forecasts were integrated with aridity concepts.
- Spatio-temporal aridity changes were presented for the future term.

## GRAPHICAL ABSTRACT



## 1. INTRODUCTION

Earth's climate is reacting to human activities conspicuously and becoming the world's most important issue to be dealt with by all countries. Climate patterns are changing day by day as a consequence of anthropogenic effects which originated from energy requirements in particular. These requirements cause greenhouse gas (GHG) emissions, hence the temperature has increasing trends in various parts of the Earth (IPCC 2013).

It is important to monitor climate change so that the relevant authorities may take measures against natural hazards such as droughts, floods, and tornados which are induced by unbalanced climatological shifts. One of them, droughts, can be defined as a normal climatological event that can occur in every type of climate regime; however, it can be more severe in arid regions (Smakhtin & Schipper 2008). In the literature, those ideas can sometimes intermingle with one another, drought and aridity. Drought is considered as a notion of temporary events, which is why it is called a natural hazard but undergone more slowly than others, whereas aridity is a long-term climate condition that generally specifies the climate state of a region. Hence, aridity is significant within the scope of climate change (Maliva & Missimer 2012).

The aridity can be indexed by means of several methods which are mainly the functions of precipitation ( $P$ ), temperature ( $T$ ), and temperature-related potential evapotranspiration ( $PET$ ). In the related literature, it is possible to encounter many downscaling implementations relevant to  $P$  and  $T$  variables. However, the number of studies concentrating on the derivation of the aridity indices from the downscaled  $P$  and  $T$  projections is rather limited (e.g. Yin *et al.* 2015; Dascălu *et al.* 2016; Lin *et al.* 2018). Moreover, several studies about the determination of aridity index ( $AI$ ) and evaluation within the scope of climate change are as follows. For instance, Marengo & Bernasconi (2015) prepared a study of climate change projections over Brazil and tried to predict the AIs until 2100 by means of a regional model integrated with the HadCM3 climate model under the A1B emission scenario. The AIs proposed by Budyko (1958) and the United Nations of Environmental Programme (UNEP) (1992) were used in their study to determine the historical and future aridity of Brazil. They estimated negative effects in terms of meteorological variables and did not detect any significant difference between the indexes until 2071. Nastos *et al.* (2013) made a projection study in Greece by means of eight regional climate models (RCMs) run under SRES A1B. They weighted the climate models with regard to their performances and obtained an ensemble model. They also utilized interrelated AIs, which were UNESCO (1979) and UNEP (1992), and found drier spells that may take place in the future for both of them. In addition to the above-mentioned studies prepared under the CMIP3 data set, there are projections derived under the CMIP5 data set. For instance, Scheff & Frierson (2015) used 16 general circulation

models (GCMs) employed under the RCP8.5 scenario and the ratio of  $P$  and  $PET$  to obtain the AI for the regions of America, India, and South Africa. They used the Penman–Monteith (PM) method to calculate  $PET$  and provided information about a possible expansion of aridity in the future. [Fernandez et al. \(2017\)](#) used the Koppen–Trewartha climate classification method to label possible climate regimes in the future and vegetation cover as well. They utilized an ensemble mean of four RCMs under RCP8.5 and found aridification signals over South America.

In fact, any aridity projection work under RCP scenarios has not been exercised for the basin of Turkey. This is one of the outstanding aspects of the study. Another novel aspect is the development of a temperature-based  $PET$  approach that simulates the PM predictions, and thus converting the RCP scenario-based  $T$  projections into  $PET$  and aridity projections. In this study, it is desired to investigate possible future AIs over the Gediz Basin, an important basin where agriculture has the biggest allocation in the production sector. The up-to-date climate models derived under IPCC's fifth assessment report, AR5, were taken into account. Three scenarios related to future GHG stabilization named as representative concentration pathways (RCPs) were utilized. Twelve GCMs under two mid-stabilization scenarios RCP4.5, RCP6.0, and a high-stabilization scenario RCP8.5 were employed. A novel methodological strategy was applied by means of downscaling/multi-model ensemble/bias-correction strategy which will be discussed in the Methodology section and the projections were obtained for the period 2015–2050. Projections that were prepared for this study have three processes: (a) downscaling of precipitation and temperature, (b) calculation of  $PET$ , and (c) estimation of AI for the term 2015–2050. The proposed methodological strategy is thought to provide a practical way for researchers interested in the subject. In the remaining part of the paper, the results which were achieved under different RCP scenarios were evaluated and finally, a conclusion with a thorough discussion about the study area is given.

## 2. STUDY AREA AND DATA

The study area is the Gediz Basin which is located in the western part of Turkey. The Gediz Basin is named after the Gediz River with a 401-km long river reach and a drainage area of 17,125 km<sup>2</sup>. The river rises from Murat Mountain of the Kutahya region in the east and flows into the Aegean Sea in the west. The study area has a typical Mediterranean climate. Most of the population existing in the basin lives off the agricultural sector. Agricultural productions are made in irrigated fields with an area of 110,000 ha which extends from south to west of the basin. In the study, the data of 20 meteorological stations which observe both  $P$  and  $T$  were utilized for the time period between January 1980 and December 2005, and the data archive is provided by the Turkish Meteorological Service (TMS) ([Table 1](#), [Figure 1](#)). According to the data, the mean areal  $P$  is observed as 550 mm per year, and the mean annual  $T$  is observed as 13 °C.

In the climate change studies, the reanalysis data which represent the atmospheric, oceanic, and land surface state of the past time are utilized frequently ([Tuel et al. 2020](#); [Krikken et al. 2021](#)). In this work, ERA-Interim reanalysis data were used so as to determine predictor variables of the Gediz Basin  $T$  and utilized as inputs in downscaling applications. The reanalysis data set covers the Gediz Basin between 37.875°–39.375°N latitudes and 26.625°–29.625°E longitudes with the resolution of 0.75° in both axes. The selected time period of the reanalysis data is the same as  $P$  and  $T$  data obtained from the TMS.

In this study, the climate scenarios referred to in IPCC's AR5 were taken into account. In AR5, RCPs in which the radiative forcing forecasts are made for the 21st century and after are constituted by means of different emission scenarios. In the work, the mid-stabilization pathways RCP4.5 and RCP6.0 and a high-stabilization pathway RCP8.5 scenarios were taken into consideration for this study. The optimistic scenario RCP2.6 where it is foreseen to have a radiative force of 2.6 W/m<sup>2</sup> by the end of 2100 was not evaluated because it is desired to seek the climate in the conditions of increasing radiative forcing and GHG emissions. The Coupled Model of Intercomparison Phase 5 (CMIP5) data set of 12 GCMs was utilized for the related RCP scenarios. Though more than 30 GCMs were present in the CMIP5 archive, some GCMs were eliminated through minding the compatibility between the variables in ERA-Interim and GCM data sets. [Anandhi et al. \(2008\)](#) and [Okkan & Inan \(2015\)](#) recommended the usage of Kendall's Tau non-parametric rank correlation statistics to detect the relationship between reanalysis predictors and historical scenario results of GCMs and expressed that this statistic has expediences comparable with other indices. In the study, the GCMs, in which the rank correlation statistics were less than or equal to 0.3, were ruled out and as a result, it was decided to utilize 12 GCMs that were also listed in [Okkan & Kirdemir \(2016\)](#). The computational details about the GCM-based rank indicators were not given in the paper due to the limitation of word number. Although it was possible to access the data of the whole of the 21st century, the projection period was decided as the years between 2015 and 2050 such that it was considered that predictions are less uncertain for the near future. Moreover, in addition to data of

**Table 1** | Meteorological stations used in the study with their spatial information

Station name	Station no.	Altitude (m)	Latitude (°) N	Longitude (°) E
Akhisar	17184	93	38.917	27.817
Alasehir	5974	189	38.350	28.517
Demirci	17746	851	39.050	28.650
Foca	5434	10	38.667	26.750
Gediz	17750	825	39.050	29.417
Golmarmara	5273	150	38.717	27.917
Gordes	4930	550	38.933	28.300
Gure	5458	650	38.650	29.167
Koprubasi	5278	250	38.750	28.400
Kula	5624	675	38.550	28.650
Manisa	17186	71	38.617	27.433
Menemen TS	9020	10	38.600	27.067
Salihli	17792	111	38.483	28.133
Sarigol	6143	225	38.250	28.700
Saruhanli	5269	50	38.733	27.567
Selendi	5282	575	38.750	28.867
Turgutlu	5615	120	38.500	27.700
Usak	17188	919	38.671	29.404
Simav	17748	809	39.093	28.979
Kemalpasa	5785	200	38.433	27.417

RCP scenarios, historical period data were utilized as the reference scenario (REF) which represents past climate over the region. The reason for the reference period for all of GCMs is commonly provided as in between 1980 and 2005, the same time period was chosen for both ERA-Interim reanalysis and observed TMS data. In GCMs, the atmospheric variables at different atmospheric levels are selected the same as those of the ERA-Interim reanalysis data set so that selected predictors via reanalysis data could be used analogously at the stage of downscaling GCMs. The related atmospheric variables that exist in both reanalysis data and GCMs are monthly mean air temperature (air), sea level pressure (slp), large-scale precipitation (pr) at surface level, mean air temperature, and geopotential height at atmospheric levels of 200, 500, and 850 hPa (air200, air500, air850, hgt200, hgt500, hgt850) and relative humidity at atmospheric levels of 500 and 850 hPa (rhum500, rhum850).

The purpose of the study is to determine the AIs of the Gediz Basin in the future. The methodology set up for this purpose requires projection of the *P* for the related time period and these data were extracted from Okkan & Kirdemir (2016) (hereinafter referred to as *OK16*). In *OK16*, the projection of *P* over the Gediz Basin was derived for RCP4.5, RCP6.0, and RCP8.5 scenarios. The information about precipitation projections prepared over the Gediz Basin will be given in the Results section. Moreover, the details of GCMs used in this study are given in Table 2.

### 3. METHODOLOGY

#### 3.1. Downscaling of GCM data

GCMs that are relatively coarse in terms of resolution are not efficient to capture the meteorological effects of climate change on the regional scale. For this reason, high-resolution results are needed to interpret the effect of coarse-resolution atmospheric models on the regional scale. Due to this requirement, it is possible to achieve a data set that more reliably represents the climatic characteristics of the study area by downscaling the coarse-resolution GCM data to the local scale using the downscaling method.

Statistical downscaling methods based on the approach of developing quantitative relations between large atmospheric variables and variables measured at the regional scale are regarded as more user-friendly tools. Besides, in a study conducted

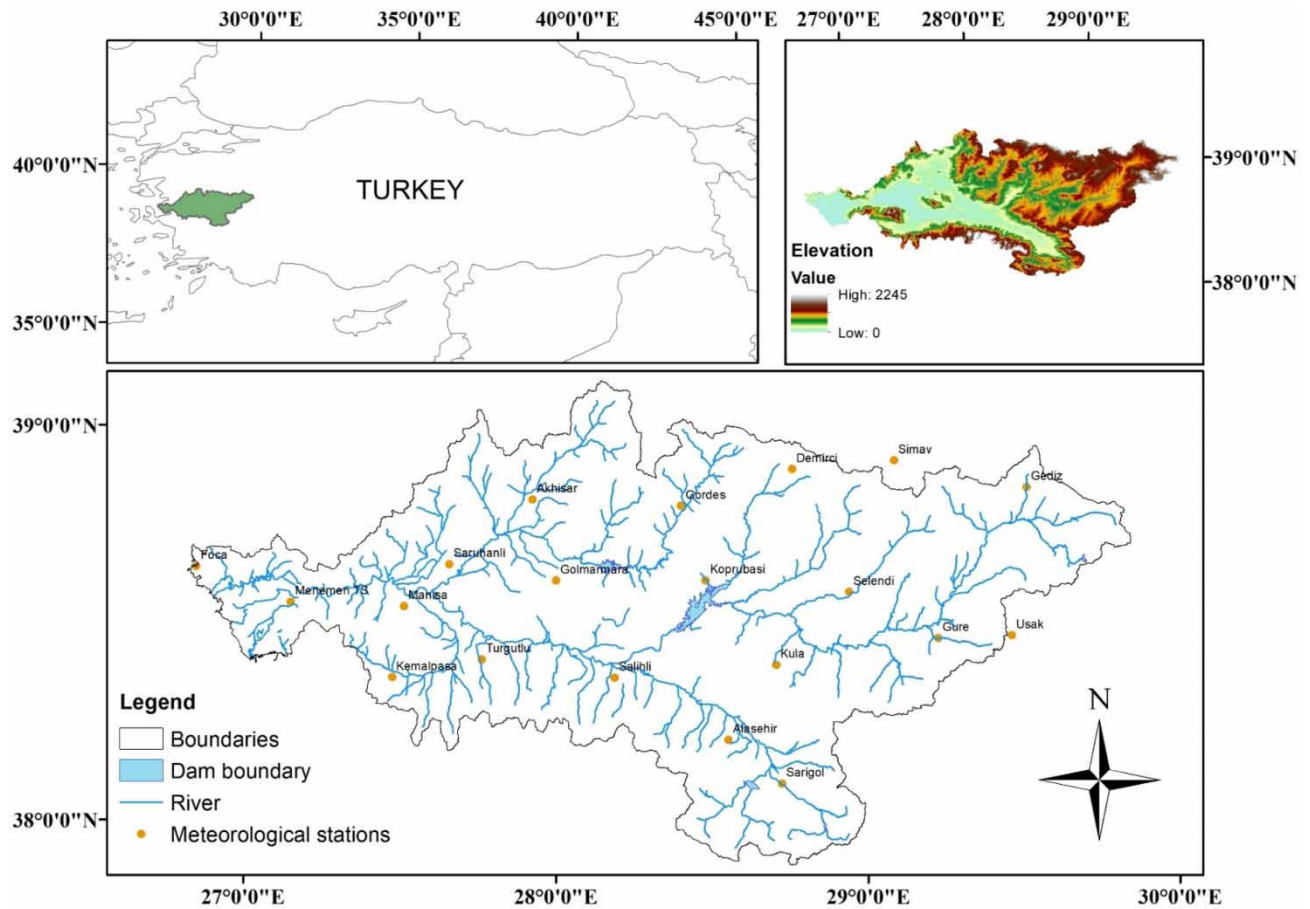


**Figure 1** | Location of the Gediz Basin and meteorological stations with digital elevation map.

in New Zealand by *Le Roux et al. (2018)*, statistical and dynamical downscaling models were compared and it was more logical to use statistical downscaling models as it demanded less computational effort although both models had close results to each other. As a consequence of these reasons, statistical downscaling methods were preferred to dynamical downscaling methods for the projections in this study. However, it should be noted that a qualified statistical downscaling model requires that various assumptions are met. These assumptions, which were earlier pointed out by *Schoof (2013)*, can be briefly listed as follows:

- There is a robust relationship between the predictors and the predictand (i.e., the variable being downscaled).
- The predictors are sufficiently simulated by the GCMs.
- The predictors incorporate the signals pertaining to climatic change.
- The relationship between the predictors and predictand shows stationary behavior.

The readers can look through the study of *Schoof (2013)* for the caveats of statistical downscaling methods and the detailed explanations about the assumptions listed above.

Artificial neural networks (ANN) and least squares support vector machines (LSSVM) methods were used for statistical downscaling to derive  $T$  projections.  $P$  projections were already obtained from *OK16*, in which  $P$  was statistically downscaled with a multi-model ensembling strategy, hence, how to get  $T$  projections will be elucidated in this study. In both downscaling methods, reanalysis variables were introduced as model inputs so that coarse-resolution GCM outputs could be downscaled to a regional scale. During the application of the downscaling models, it is aimed to define predictor sets representing the observed  $T$  in the study area in order to reduce the computational cost (*Fistikoglu & Okkan 2011*). To apply this the all possible regressions (APREG) method was used and 12 ERA-Interim reanalysis variables as predictors and  $T$  observations of 20



**Table 2** | The information of utilized GCMs

GCM name	Institution	Modeling center	Resolution Latitude (°) × Longitude (°)		Center coordinates of used grids that cover the study area
BCC-CSM1	Beijing Climate Center, China Meteorological Administration, China	BCC	1.121 × 1.125	[38.69 °N, 27 °E];	[38.69 °N, 28.125 °E]; [38.69 °N, 29.25 °E]
CCSM4	National Center for Atmospheric Research, USA	NCAR	0.942 × 1.25	[38.17 °N, 27.5 °E];	[38.17 °N, 28.75 °E]; [39.11 °N, 28.75 °E]; [39.11 °N, 27.5 °E]
CESM1 (CAM5)	National Center for Atmospheric Research, USA	NCAR	0.942 × 1.25	[38.17 °N, 27.5 °E];	[38.17 °N, 28.75 °E]; [39.11 °N, 28.75 °E]; [39.11 °N, 27.5 °E]
CSIRO- Mk3.6	Commonwealth Scientific and Industrial Research Organisation, Australia	CSIRO- QCCCE	1.865 × 1.875	[38.24 °N, 26.25 °E];	[38.24 °N, 28.125 °E]; [38.24 °N, 30 °E]
GFDL-CM3	Geophysical Fluid Dynamics Laboratory, USA	NOAAGFDL	2 × 2.5	[39 °N, 26.25 °E];	[39 °N, 28.75 °E]
GFDL- ESM2M	Geophysical Fluid Dynamics Laboratory, USA	NOAAGFDL	2.022 × 2.5	[37.416 °N, 26.25 °E];	[37.416 °N, 28.75 °E]; [39.438 ° N, 28.75 °E] [39.438 °N, 26.25 °E]
GISS-E2-H	NASA Goddard Institute for Space Studies, USA	NASA GISS	2 × 2.5	[39 °N, 26.25 °E];	[39 °N, 28.75 °E]
GISS-E2-R	NASA Goddard Institute for Space Studies, USA	NASA GISS	2 × 2.5	[39 °N, 26.25 °E];	[39 °N, 28.75 °E]
HadGEM2- ES	Met Office Hadley Centre, UK	MOHC	1.25 × 1.875	[38.75 °N, 26.25 °E];	[38.75 °N, 28.125 °E]; [38.75 °N, 30 °E]
IPSL-CM5A- LR	Institut Pierre-Sim on Laplace, France	IPSL	1.895 × 3.75	[38.842 °N, 26.25 °E];	[38.842 °N, 30 °E]
MROC-ESM	Atmosphere and Ocean Research Institute, Japan	MIROC	2.791 × 2.813	[37.673 °N, 28.125 °E]	
MRI-CGCM3	Meteorological Research Institute, Japan	MRI	1.12 × 1.125	[38.69 °N, 27 °E];	[38.69 °N, 28.125 °E]; [38.69 °N, 29.25 °E]

meteorological stations as predictands were utilized in the related method. As a result, it was deduced that it was sufficient to use the air variable (surface temperature) of the reanalysis data as the  $T$  predictor of the stations. As with this study, only the precipitation rate (prate) variable was selected as a potential predictor of  $P$  in *OK16* so it can be evaluated that prate and air variables of the ERA-Interim data set are prominent in representing  $P$  and  $T$  for the Gediz Basin.

Performance of downscaling models was evaluated by means of statistical performance criteria such as determination coefficient ( $R^2$ ),  $RMSE$ ,  $RSR$  which is the proportion of  $RMSE$  to standard deviation of observed data, and percent of bias ( $PBIAS$ ) which is the metric of overestimation or underestimation. The theoretical knowledge about the related performance criteria is detailed in *Moriasi et al. (2007)*.

### 3.2. Multi-model ensemble and bias-correction strategy

When the climate models are taken into consideration, it can be stated that they have effective roles in projecting the future climate. Even if they are practical tools for climate scientists, uncertainty still exists about the extent to which a single climate model can represent the climate of the related region. Regarding this issue, it was recommended by *IPCC (2010)* that a combination of multiple GCM results can be applied in climate projection studies by averaging or weighting the model predictions. Besides, *Kwon et al. (2010)* compared several ensemble results of  $T$  projections over East Asia and they achieved more feasible and explanatory results with a weighted ensemble model which were obtained by using Bayesian Model Averaging (BMA). Moreover, *Yang et al. (2012)* prepared a study for Tibetan Plateau and evaluated BMA and arithmetic mean method (equally weighted) for multi-model ensemble projections and they obtained more consistent results with BMA in comparison with the arithmetic mean method. Similarly, better performing results obtained by utilizing BMA were presented

in [Min et al. \(2007\)](#) and [Miao et al. \(2013\)](#), in which BMA-weighted and equally weighted results were compared. Moreover, *OK16* employed BMA for *P* projections over the Gediz Basin and derived simulations with higher significance levels than those of individual models. In the light of this information, the use of the BMA method was decided by the authors for *T* projections in the study.

[Raftery et al. \(2005\)](#) proposed BMA to reduce uncertainty in model selection by combining multi-model forecasts. The model depends on a weighting of the probability density function (PDF) of each individual model forecast; subsequently, the weighted-average forecast PDFs can be derived. In the model, the PDF of a combined forecast  $y$  is defined depending on the observed data with data size  $T$  ( $D = [y_{obs1}, \dots, y_{obsT}]$ ) and  $K$ -model forecasts ( $f_k$ ) as follows:

$$p(y|D) = \sum_{k=1}^K p(f_k|D) \cdot p_k(y|f_k, D) \quad (1)$$

where  $p(f_k|D)$  is the posterior probability of  $k$ th model forecast for given observed data and defined as a weight of the  $k$ th model ( $w_k$ ). The sum of the related model weights adds up to 1. The conditional PDF  $p_k(y|f_k, D)$  is assumed to be normally distributed and centered at the linear regression function of  $a_k + b_k \cdot f_k$  whose response variables are the observed ones. The expected value of BMA forecasts is given in Equation (2).

$$E[y|D] = \sum_{k=1}^K p(f_k|D) \cdot E[p_k(y|f_k, D)] = \sum_{k=1}^K w_k \cdot f_k \quad (2)$$

[Raftery et al. \(2005\)](#) recommended maximization of the log-likelihood function as an objective function to define the parameters which are weights ( $w_k$ ) and variances of model forecasts ( $\sigma_k^2$ ). The log-likelihood function is

$$l(\theta) = l(w_1, \dots, w_k; \sigma_1, \dots, \sigma_k) = \log \left[ \sum_{k=1}^K w_k \cdot g(y|f_k, \sigma_k) \right] \quad (3)$$

where  $g(y|f_k, \sigma_k)$  is the conditional PDF of  $y$  for given model forecasts and predicted variance. The term  $g(y|f_k, \sigma_k)$  is similar to  $p_k(y|f_k, D)$  such that it is normally distributed as  $N(a_k + b_k \cdot f_k, \sigma_k)$ . For calculation convenience of log-likelihood maximization, the expectation-maximization (EM) procedure is employed. For a detailed explanation of BMA and EM, readers are referred to [Raftery et al. \(2005\)](#).

Undoubtedly, the forecasts obtained after weighting the results of GCMs (either coarse or downscaled) cannot be completely trusted. But yet, according to [Murphy et al. \(2004\)](#) and [Chen et al. \(2017\)](#), assigning weights, and thus reducing the influence of some GCMs which do not perform as well as others, can help diminish the uncertainties stemmed from projecting stages. In connection with this issue, [Smith & Chandler \(2010\)](#) and [Whetton et al. \(2007\)](#) expressed that a model's facility to reflect past climates could be an essential criterion for simulating future climates. In this respect, weighting the individual models with respect to REF is an appropriate strategy for scenario period simulations.

The GCMs which are utilized in the study differ from each other with regard to the capability of forecasting the climate for different time periods. For example, one can be better at predicting hot seasons whereas the other can be better at predicting cold seasons. Hence, observed *T* data and downscaled REF data were divided into dry (from April to September) and wet (from October to March) periods. Thus, 12 weights belonging to 12 GCMs for each separate period were obtained in each ensemble projection of the related meteorological station. The determined weights were integrated with three RCP scenarios separately. Moreover, it is possible to interpret the prediction capabilities of GCMs after the determination of GCM weights, that is, better performing GCMs get higher weights in comparison to the other GCMs. Thus, probabilistic performances of climate models used in the study were evaluated and presented in the Results section.

There is another problem in the use of GCMs in that these models have inherent biases. [Li et al. \(2010\)](#) stated in their study that the complicated structure of the atmosphere system and converting it to a more simplified model entail GCM biases. Although the climate models have been improved in the AR5 since the AR4, according to [IPCC \(2013\)](#), biases in *T* and *P* still exist in certain climate models. Moreover, statistical downscaling models such as ANN and LSSVM have the only aim that is to calibrate the related downscaling model parameters to minimize the error value. These models do not

reckon with the reference climate properties and inherent biases of GCMs are not corrected consequently. Hence, a bias-correction procedure was applied for all downscaled and ensemble projections to derive physically and climatologically plausible simulations.

To apply the bias-correction procedure, the equidistant quantile mapping (EDQM) method which reckons cumulative distribution functions (CDFs) of data to reduce the bias values resulting from simulations. The EDQM method takes into account two factors in addition to the uncorrected projected model value to get the corrected one as follows:

$$Y_{corr,i} = Y_{scn,i} + Factor_1 - Factor_2 \quad (4)$$

where  $Y_{corr,i}$  is the bias-corrected value of the corresponding variable on the  $i$ th month for the related scenario,  $Y_{scn,i}$  is the uncorrected value of the corresponding variable on the  $i$ th month for the related scenario ( $scn$ ). The  $Factor_1$  and  $Factor_2$  are calculated as

$$Factor_1 = F^{-1}(F(Y_{scn,i}, \theta_{scn,i}), \theta_{observed,i}) \quad (5)$$

$$Factor_2 = F^{-1}(F(Y_{scn,i}, \theta_{scn,i}), \theta_{historical,i}) \quad (6)$$

where CDF of each scenario value for the related month with respect to distributional function and parameters are obtained in both factors. EDQM is sharply separated from the quantile mapping (QM) method with this property, such that EDQM reckons with distributional parameters of both historical and future scenarios whereas QM takes into account the CDFs only with respect to the distribution of historical scenario and maps onto the observed one. The CDFs of each simulation on the related month are calculated by using PDF as follows:

$$F(Y_{scn,i}; \theta_{scn,i}) = \int_{-\infty}^{Y_{scn,i}} f(x; \theta_{scn,i}) dx \quad (7)$$

where  $f(x; \theta_{scn,i})$  is the PDF of a corresponding meteorological variable for given distribution parameters. Also,  $F^{-1}(\cdot)$  represents the inverse CDF and  $\theta_{historical,i}$  and  $\theta_{observed,i}$  denotes the value of the distribution parameters of a corresponding meteorological variable for the historical scenario and observed data, respectively.

The above-mentioned corresponding meteorological variable is  $T$  for this study. The bias-corrected time series of  $P$  was already obtained from *OK16*. The EDQM method requires fitting distribution functions for the time series, hence, the probability plot-correlation coefficient (PPCC) tests were applied to observe and downscaled  $T$  time series. As a result of the PPCC tests, it was determined that  $T$  time series were fitted to a normal distribution, so the distribution parameters were mean and standard deviation for this application. For the sake of brevity, the results of the PPCC tests will not be given in the study.

### 3.3. Simulation of PET and AI

In the literature, there are several methods used for determination of the  $AI$ . Most of them determine the  $AI$  by using  $P$ ,  $PET$ , or  $T$  data. One of them is the  $P$  and  $T$  data user Köppen and Trewartha climate classification method which is used for the definition of climate regime and prevalent vegetation type related to the climatic conditions. Another method is De Martonne's  $AI$  method in which  $AI$  is calculated with a proportion of mean annual  $P$  to mean annual  $T$  plus  $10^\circ\text{C}$ . The difference between mean annual  $PET$  and mean annual  $P$  over mean annual  $P$  is defined as Thornthwaite  $AI$ . Similarly, UNESCO (1979) expressed  $AI$  as the proportion of mean annual  $P$  to mean annual  $PET$ , and the same proportion was proposed by UNEP (1992). The difference between UNESCO (1979) and UNEP (1992) is the method of definition of  $PET$ . In UNESCO (1979)  $PET$  is defined by using the standard Penman formula, while  $PET$  is defined by using Thornthwaite empirical equations in UNEP (1992). Different from those,  $AI$  is defined with mean annual net radiation, mean annual  $P$ , and latent heat of evaporation by Budyko (1958). Upon examining the above-mentioned methods, they reflect correlative properties (Paltineanu *et al.* 2007), hence, in the study, it was found adequate to use UNEP (1992)  $AI$  for the calculation of  $AI$  by

$$AI = \frac{P}{PET} \quad (8)$$



As mentioned above, *PET* is calculated by means of the Thornthwaite formula in UNEP (1992). However, in the literature, the PM method is introduced as a standard *PET* calculation method such that it is considered as an indirect measurement of *PET* besides lysimeter measurements. Although the PM method is taken into consideration as the standard reference method, it can be unfeasible in certain regions due to the fact that PM requires a large amount of data. It demands data such as average dew point temperature, several variants of radiation, pressure, and wind speed such that they are highly possible to be unmeasured in a region or it is not possible to obtain them as continuously measured. The lack of input data of PM is problematic for the Gediz Basin, too, hence it was decided to extract ERA-Interim reanalysis data sets required for *PET* calculation by PM. Okkan & Kiyamaz (2019) already revealed that several input data of PM obtained from reanalysis data sets are compatible to observed data in the Gediz Basin, thus, it is considered that reanalysis data sets have enough spatio-temporal reliability in terms of compatibility to actual data of the Gediz Basin. In order to project *PET* in accordance with RCPs, the PM method was simulated by calibrating coefficients of temperature-based Hamon (Ham), Blaney–Criddle (Bl–Cr), and Thornthwaite (Thw) methods, and the performance of the best method was utilized for *PET* projections. The input of outperforming method is *T* projections derived under RCPs. Subsequently, AI and climatic regimes were defined for REF and scenario period, separately. To give an example, similar coefficient adjustment practices were also implemented for radiation-based *PET* methods such as Hargreaves and Priestley–Taylor equations as in Tabari & Talaei (2011). The climatic regimes corresponding to AI intervals are listed in Table 3.

## 4. RESULTS

### 4.1. Possible changes in temperature

#### 4.1.1. Statistical downscaling phase

In the study, the projection studies were initialized by downscaling coarse-resolution reanalysis and GCM data to a local scale. Prior to the downscaling, the time series of potential predictor and local-scale temperature were divided into equal time periods for training and testing the models. When the results of ANN and LSSVM were compared, it was realized that the statistical performances of both models were close to each other in the training phase. Hence, the decision was made about which downscaling model results to be used in terms of testing performances due to the fact that extrapolation capabilities of models are prominent in climate studies (Table 4). Subsequent to the determination of related parameters of better performing downscaling models, they were integrated with data of REF and RCP scenarios. Upon assessing the test results of the models for each station, both ANN and LSSVM models show ‘very good’ testing results at downscaling *T* for each station in terms of *NS*, *RSR*, and *PBIAS* (please check qualitative evaluations of performance criteria from Moriasi *et al.* (2007)). In the decision phase of model selection, test results of better performing models were selected and utilized in the next process.

#### 4.1.2. Multi-model ensemble, bias correction, and ultimate results

In the downscaling application, the raw GCM data were integrated with calibrated and validated downscaling models which were selected individually for each station and it was obtained that the statistical behavior of *T* series belonging to 12 GCMs was different from each other. As stated before, this situation entails uncertainty in model selection and puts trouble in the decision. Hence, the BMA method was utilized to produce weighted-average projections in which 12 GCMs were combined.

**Table 3** | Climatic zones corresponding to AI

AI	Climatic zone	Acronym
<0.05	Hyper-Arid	HA
0.05–0.20	Arid	A
0.20–0.50	Semi-Arid	SA
0.50–0.65	Dry Sub-Humid	DSH
0.65–1.00	Sub-Humid	SH
1.00–2.00	Humid	H
>2.00	Hyper-Humid	HH

**Table 4** | Testing performances of ANN and LSSVM as temperature downscaling models

Stations	ANN					LSSVM					Selected downscaling model	
	n.n.h	$R^2$	NS	RSR	PBIAS (%)	$\gamma$	$\sigma$	$R^2$	NS	RSR		PBIAS (%)
Akhisar	3	<u>0.9931</u>	<u>0.9909</u>	<u>0.0948</u>	<u>1.82</u>	2.29E + 05	0.80	0.9929	0.9905	0.0974	2.02	ANN
Alasehir	2	0.9899	0.9891	0.1040	1.19	2.32E + 05	3.18	<u>0.9899</u>	<u>0.9892</u>	<u>0.1037</u>	<u>1.15</u>	LSSVM
Demirci	4	0.9892	<u>0.9887</u>	<u>0.1061</u>	<u>1.15</u>	1.73E + 05	31.91	<u>0.9896</u>	0.9886	0.1062	1.69	ANN
Foca	6	0.9918	0.9902	0.0986	0.35	8.62E + 02	0.55	<u>0.9921</u>	<u>0.9905</u>	<u>0.0970</u>	<u>0.31</u>	LSSVM
Gediz	15	0.9913	0.9910	0.0945	<u>0.92</u>	1.35E + 06	23.85	<u>0.9915</u>	<u>0.9911</u>	<u>0.0938</u>	<u>0.99</u>	LSSVM
Golmarmar	3	0.9910	<u>0.9908</u>	<u>0.0957</u>	<u>0.22</u>	6.31E + 04	0.71	<u>0.9928</u>	0.9900	0.0995	2.10	ANN
Gordes	3	0.9905	0.9899	0.1002	0.35	3.86E + 02	2.73	<u>0.9907</u>	<u>0.9903</u>	<u>0.0980</u>	<u>0.09</u>	LSSVM
Gure	5	0.9887	0.9886	0.1065	- 0.15	6.50E + 07	49.21	<u>0.9888</u>	<u>0.9888</u>	<u>0.1057</u>	<u>0.15</u>	LSSVM
Kemalpasa	4	0.9926	0.9925	0.0863	- 0.25	6.93E + 02	0.54	<u>0.9930</u>	<u>0.9925</u>	<u>0.0861</u>	<u>- 0.15</u>	LSSVM
Koprubasi	3	0.9857	0.9852	0.1214	0.87	1.03E + 08	2.67	<u>0.9857</u>	<u>0.9853</u>	<u>0.1210</u>	<u>0.78</u>	LSSVM
Kula	6	0.9898	0.9892	0.1036	<u>0.45</u>	1.30E + 02	2.60	<u>0.9900</u>	<u>0.9894</u>	<u>0.1028</u>	0.66	LSSVM
Manisa	1	0.9930	0.9924	0.0868	<u>0.02</u>	8.26E + 02	0.55	<u>0.9936</u>	<u>0.9927</u>	<u>0.0852</u>	0.02	LSSVM
Menemen	6	<u>0.9787</u>	<u>0.9629</u>	<u>0.1920</u>	<u>4.85</u>	6.84E + 02	0.56	0.9786	0.9622	0.1939	4.96	ANN
Salihli	6	<u>0.9930</u>	<u>0.9914</u>	<u>0.0924</u>	<u>1.23</u>	4.28E + 05	3.59	0.9930	0.9912	0.0937	1.50	ANN
Sarigol	6	<u>0.9931</u>	<u>0.9913</u>	<u>0.0927</u>	<u>1.42</u>	1.31E + 04	2.48	0.9929	0.9912	0.0937	1.51	ANN
Saruhanli	3	0.9929	0.9910	0.0944	<u>1.65</u>	2.85E + 06	4.66	<u>0.9933</u>	<u>0.9914</u>	<u>0.0927</u>	1.77	LSSVM
Selendi	3	0.9932	0.9926	0.0860	- 0.08	3.30E + 02	0.62	<u>0.9934</u>	<u>0.9928</u>	<u>0.0848</u>	<u>- 0.02</u>	LSSVM
Simav	6	<u>0.9919</u>	<u>0.9897</u>	<u>0.1013</u>	<u>2.57</u>	4.74E + 06	5.27	0.9919	0.9894	0.1027	2.89	ANN
Turgutlu	3	0.9903	0.9894	0.1027	<u>0.49</u>	1.39E + 06	0.87	<u>0.9906</u>	<u>0.9896</u>	<u>0.1017</u>	0.50	LSSVM
Usak	4	0.9931	0.9930	0.0831	<u>0.09</u>	7.41E + 03	30.20	<u>0.9932</u>	<u>0.9932</u>	<u>0.0824</u>	0.26	LSSVM

Better performing results are underlined.

n.n.h., number of neurons in hidden layer;  $\gamma$ , regularization parameter;  $\sigma$ , RBF width.

For each station, observed data and historical projections of 12 GCMs were utilized and the time series were divided into wet and dry periods. In this process, each GCM had its own weight for wet and dry periods, respectively. In the end, the expected values of multi-model ensembles for related wet and dry periods were derived and the long-term monthly time series were reproduced by combining wet and dry periods. Same weights were used for RCP4.5, RCP6.0, and RCP8.5 scenarios, respectively. The related weights are shown in Table 5 for each meteorological station. According to Table 4, BCC-CSM1.1 and HADGEM2-ES climate models have the highest weight values for wet and dry periods, respectively. Due to the fact that the better the model performs, the higher the weight value it gets, it can be interpreted that BCC-CSM1.1 and HADGEM2-ES climate models have the highest capability of representing the local temperature over the Gediz Basin for wet and dry periods, respectively.

Of course, in addition to BMA, the simple model averaging (SMA) method is also frequently used in climate change studies in order to get GCM ensembles (Miao *et al.* 2013; Wang *et al.* 2018). In the study, Mann-Whitney *U* tests were utilized so that a comparison could be made between BMA and SMA. Dibike *et al.* (2007) proposed the Mann-Whitney *U* test to perform uncertainty analysis for GCMs in which it was investigated if the medians of REF time series of GCMs and observed time series were statistically equal. In this study, a similar aspect was conformed for comparison of BMA and SMA ensemble results. The non-parametric test analyses were done for monthly and annual time scales and the evaluations were made in terms of quantity of confidence levels ( $1 - p$  value). According to the confidence levels, it was realized that the BMA method had dominance over both SMA and single GCMs for a major part of the time scales. However, in several months (such as March and October for the Alasehir station) SMA had slightly better performance in comparison to BMA. Moreover, in some months (such as March, April, and June for the Alasehir station) the single GCMs such as GFDL-ESM2M, MIROC-ESM, Csiro-Mk3.6, and CCSM4 had higher levels than those of ensemble levels. Generally, it can be stated that the BMA

**Table 5** | The weights of each GCM obtained for the meteorological stations

Stations	Periods	BCC-CSM1.1	CCSM4	CESM1(CAM5)	Csro-Mk3.6	GFGL-CM3	GFGL-ESM2M	GISS-E2-H	GISS-E2-R	HADGEM2-ES	IPSL-CM5A-LR	MIROC-ESM	MRI-CGCM3
Akhisar	Wet	0.095	0.082	0.086	0.088	0.078	0.076	0.085	0.086	0.076	0.086	0.086	0.076
	Dry	0.080	0.079	0.088	0.092	0.077	0.082	0.073	0.089	0.111	0.077	0.082	0.069
Alasehir	Wet	0.096	0.083	0.087	0.083	0.077	0.074	0.088	0.086	0.078	0.085	0.085	0.077
	Dry	0.082	0.078	0.088	0.097	0.078	0.081	0.073	0.082	0.108	0.078	0.082	0.073
Demirci	Wet	0.098	0.087	0.087	0.087	0.075	0.074	0.079	0.084	0.076	0.089	0.085	0.078
	Dry	0.080	0.076	0.085	0.098	0.077	0.080	0.075	0.082	0.105	0.083	0.083	0.075
Foca	Wet	0.098	0.078	0.086	0.082	0.078	0.080	0.082	0.084	0.076	0.090	0.089	0.077
	Dry	0.079	0.077	0.090	0.097	0.076	0.082	0.071	0.083	0.115	0.077	0.083	0.069
Gediz	Wet	0.092	0.080	0.087	0.085	0.079	0.074	0.086	0.087	0.080	0.085	0.085	0.080
	Dry	0.079	0.080	0.086	0.094	0.082	0.076	0.074	0.082	0.106	0.084	0.082	0.075
Golmarmara	Wet	0.091	0.083	0.085	0.087	0.080	0.077	0.084	0.087	0.079	0.084	0.086	0.077
	Dry	0.081	0.082	0.086	0.093	0.075	0.084	0.072	0.087	0.114	0.075	0.085	0.068
Gordes	Wet	0.094	0.078	0.086	0.087	0.075	0.077	0.083	0.087	0.077	0.089	0.087	0.078
	Dry	0.077	0.078	0.088	0.094	0.078	0.078	0.072	0.084	0.109	0.079	0.085	0.077
Gure	Wet	0.094	0.081	0.085	0.083	0.079	0.075	0.087	0.089	0.080	0.082	0.086	0.079
	Dry	0.082	0.079	0.086	0.095	0.082	0.078	0.074	0.082	0.104	0.083	0.082	0.074
Kemalpasa	Wet	0.094	0.080	0.087	0.086	0.076	0.078	0.084	0.086	0.077	0.088	0.086	0.077
	Dry	0.080	0.078	0.086	0.095	0.076	0.083	0.075	0.085	0.112	0.077	0.082	0.070
Koprubasi	Wet	0.094	0.079	0.088	0.086	0.075	0.077	0.081	0.089	0.076	0.090	0.087	0.078
	Dry	0.081	0.078	0.089	0.093	0.075	0.078	0.073	0.086	0.109	0.084	0.082	0.072
Kula	Wet	0.090	0.082	0.084	0.088	0.077	0.079	0.085	0.090	0.077	0.086	0.084	0.079
	Dry	0.078	0.078	0.087	0.091	0.079	0.083	0.077	0.089	0.109	0.077	0.081	0.071
Manisa	Wet	0.093	0.080	0.086	0.087	0.077	0.078	0.084	0.087	0.078	0.087	0.086	0.078
	Dry	0.080	0.078	0.086	0.095	0.077	0.083	0.074	0.085	0.112	0.077	0.083	0.071
Menemen	Wet	0.094	0.080	0.084	0.083	0.078	0.078	0.082	0.090	0.078	0.087	0.089	0.076
	Dry	0.081	0.083	0.087	0.090	0.074	0.086	0.079	0.091	0.100	0.077	0.083	0.069
Salihli	Wet	0.094	0.084	0.085	0.085	0.077	0.076	0.085	0.090	0.079	0.082	0.087	0.077
	Dry	0.081	0.066	0.086	0.093	0.075	0.077	0.081	0.092	0.116	0.077	0.079	0.077
Sarigol	Wet	0.094	0.082	0.085	0.088	0.077	0.077	0.084	0.089	0.078	0.083	0.085	0.077
	Dry	0.080	0.079	0.087	0.093	0.077	0.082	0.078	0.089	0.110	0.076	0.080	0.071
Saruhanli	Wet	0.094	0.083	0.086	0.088	0.077	0.075	0.084	0.088	0.077	0.082	0.086	0.078
	Dry	0.080	0.078	0.086	0.091	0.076	0.084	0.077	0.089	0.111	0.076	0.081	0.071
Selendi	Wet	0.092	0.079	0.084	0.086	0.076	0.080	0.084	0.088	0.078	0.087	0.085	0.081
	Dry	0.081	0.080	0.087	0.095	0.076	0.083	0.075	0.083	0.106	0.079	0.086	0.070
Simav	Wet	0.097	0.083	0.087	0.088	0.078	0.074	0.083	0.086	0.076	0.085	0.088	0.076
	Dry	0.081	0.080	0.087	0.094	0.077	0.082	0.075	0.087	0.108	0.076	0.082	0.071
Turgutlu	Wet	0.093	0.081	0.086	0.087	0.078	0.080	0.082	0.088	0.077	0.086	0.085	0.078
	Dry	0.079	0.070	0.086	0.094	0.077	0.083	0.077	0.091	0.112	0.077	0.080	0.074
Usak	Wet	0.095	0.081	0.084	0.085	0.076	0.074	0.085	0.088	0.079	0.089	0.088	0.077
	Dry	0.080	0.078	0.088	0.093	0.078	0.080	0.074	0.085	0.105	0.082	0.083	0.074

Maximum values are coloured for wet and dry periods separately.

method had more confident results than those of SMA and single GCMs, hence it makes sense to use BMA ensembles in further projections such as *PET* and *AI*. In Figure 2, the confidence levels obtained by Mann–Whitney *U* tests were presented for the Alasehir station. Similar results were encountered in other stations as well. However, the decomposition of total uncertainty in RCP-based projections was not addressed in the study. In other words, supposing that the projection is made up of three stages applied (i.e., GCMs, emission scenarios, and downscaling models), it has not been identified how uncertainties are propagated as the stages proceed in produced projections. The above-mentioned uncertainty analysis used in the study was only performed for the REF, similar to that in Dibike *et al.* (2007).

Subsequent to a combination of 12 GCM results, the EDQM method was utilized to eliminate the model biases. As seen in the sample of the Foca meteorological station, the uncorrected REF simulation has different statistics and frequency distribution when compared to the observed time series (Figure 3(a) and 3(b)). In order to capture the climatological conditions of the study area, the model biases were corrected and it was obtained that the corrected historical *T* series were more compatible to the observed series (Figure 3(c)). Similar biased results were produced for other related meteorological stations and the related bias-correction procedure were applied for all of them.

Upon evaluating the *T* projections for all meteorological stations, it is foreseen that mean annual *T* changes between +1.26 and +2.80 °C may occur over different regions of the Gediz Basin. The maximum mean annual *T* increases for all concentration pathways are predicted in Salihli meteorological station as +1.94, +1.95, and +2.80 °C for RCP4.5, RCP6.0, and RCP8.5, respectively. When the possible spatial changes in *T* are evaluated over the Gediz Basin, it is obtained that the highest changes for all RCPs are expected in the southern part of the basin and this situation spreads to the mid-northern part of the basin. In the eastern part of the basin, the expected temperature changes are around the calculated mean annual changes for the entire basin (1.54, 1.60, and 2.18 °C for RCP4.5, RCP6.0, and RCP8.5, respectively). Upon evaluating the westward change of *T* increase, especially in the central part of the basin, the related amount of expected increase diminishes gradually.



**Figure 2 |** Mann-Whitney *U* confidence levels of GCMs and ENSEMBLE results for monthly and annual time scales. In the bar charts, the vertical axis stands for confidence levels (between 0 and 1) and horizontal axis stands for GCMs and ensemble models.

For the entire basin, the mean annual *T* which is about 15.1 °C in the REF is foreseen that it may increase to 16.7, 16.8, and 17.3 °C for RCP4.5, RCP6.0, and RCP8.5, respectively. In addition to an annual analysis of possible *T* changes, they were assessed in terms of seasonal periods. According to this assessment, the highest increase is expected in the summer season for all RCPs. The mean summer *T* which is about 25 °C in the reference period may increase by 1.87, 1.74, and 2.46 °C for RCP4.5, RCP6.0, and RCP8.5, respectively. In autumn seasons, the mean *T* of 15.9 °C may increase by 1.52, 1.62, and 2.44 °C for RCP4.5, RCP6.0, and RCP8.5, respectively. The mean spring *T* is expected to increase 1.44, 1.52, and 1.99 °C, and the mean winter *T* may increase 1.34, 1.52, 1.85 °C for RCP4.5, RCP6.0, and RCP8.5, respectively. In the seasonal evaluation, it is realized that the temperature increase is directly proportional with respect to radiative forcing for the winter, spring, and autumn seasons while the mean temperature of RCP4.5 is higher than the mean temperature of RCP6.0 for the summer season. Similar predictions were experienced in the monthly evaluations of *T* projections as well. The maximum *T* increase for both RCP6.0 and RCP8.5 is expected in October as 1.88 and 2.68 °C, respectively, but in August for RCP4.5 as 2.03 °C (Figure 4). In the study, hypothesis testing was made on whether the mean annual, seasonal and monthly *T* changes are significant with respect to REF temperature of the related time periods. To do this, two sample *t*-tests were applied for the mean values of the projected *T* series of annual, seasonal, and monthly time periods (the significance level is 0.05).



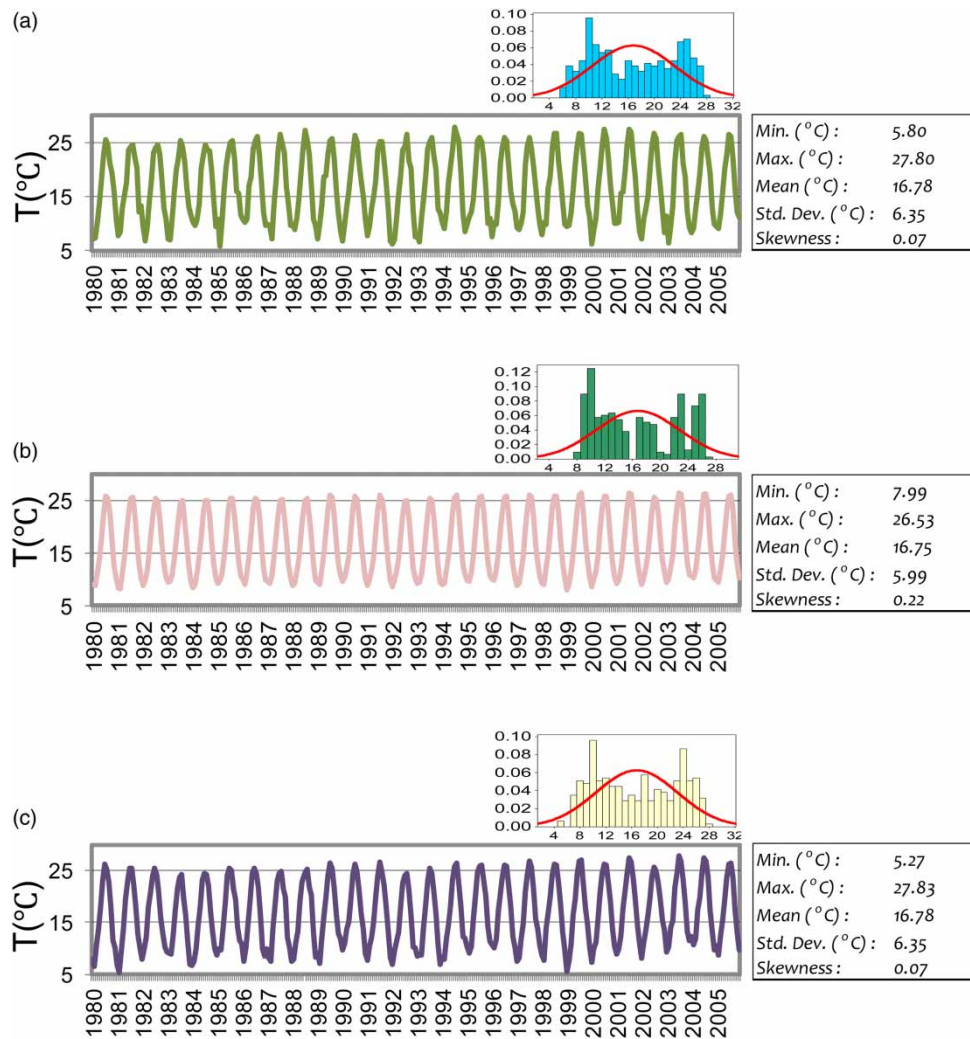


**Figure 3** | (a) Time series of Foca meteorological station plotted for observed temperature, (b) downscaled but uncorrected historical scenario temperature and (c) downscaled and corrected historical scenario temperature. The histograms at the upper-right corner of the graphs show the frequency as percentile in the vertical axis and temperature in the horizontal axis with the distribution curves.

Consequently, it was deduced that all possible changes are statistically significant with respect to historical  $T$  for annual, seasonal and monthly time periods until 2050.

#### 4.2. Possible changes in $PET$

Similar assessments for  $T$  projections were made for  $PET$  forecasts which were projected through T-based empirical equations modified in accordance with the PM method. In order to handle the provision of input data demanded by the PM method, ERA-Interim reanalysis data sets were utilized and  $PET$  estimations were obtained for the past period. In  $PET$  simulations, the observed PM data were simulated by means of three different  $PET$  methods which relied on Ham, Thw, and Bl-Cr methods such that they commonly use temperature data as input. Ham, Bl-Cr, and Thw-based  $PET$  equations were modified by adjusting the coefficients of the formulas depending on PM estimations so that  $PET$  estimations were derived for RCP scenarios by integrating  $T$  projections into adjusted T-based formulas. The formulas for simulation models are presented in Table 6. The parameters in the related formulas were already optimized by the model developers, for instance, a, b, c, and d were 0.6915, 2, 0.062, and 0 for the original Ham method, respectively. However, it was thought that these parameters can deviate with respect to the climate of the study region (see Xu & Singh 2001; Okkan & Kiyamaz 2019), so the parameters for each model were calibrated for each station in the Gediz Basin again. In this process, the data were divided into calibration



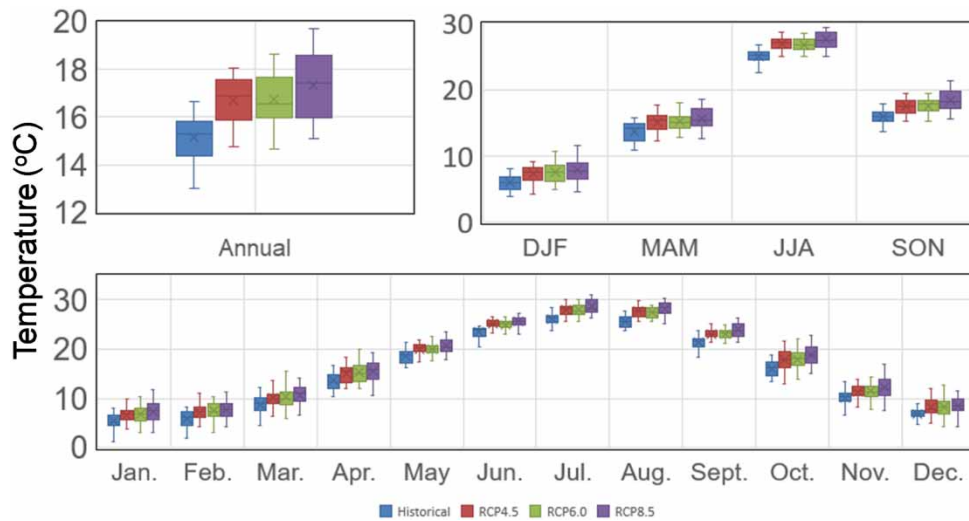


**Figure 4** | Box-plots of mean annual, seasonal, and monthly temperature projected under historical, RCP4.5, RCP6.0, and RCP8.5 scenarios. The acronyms DJF, MAM, JJA, and SON denote winter, spring, summer, and autumn seasons, respectively. The labels in the horizontal axis of the seasonal box-plots are the initial letters of the months composing the related seasons.

and verification data with equal ratios, and the statistical performances were presented in accordance with time series containing both calibration and verification predictions. The level of biases of the predictions derived from recalibrated equations against the PM predictions was questioned by criteria such as  $R^2$ ,  $NS$ , and  $RSR$ , which were also assessed in the investigations of downscaling model performances. It was found unnecessary to give the  $PBIAS$  results due to the fact that each model derived  $PBIAS$  values close to zero. As a result of the calibrations carried out separately on 20 meteorological stations, it is deduced that the predictions of the modified Ham equation adequately represent those of the reference method in terms of several performance measures denoted in Table 6. Then, the T-based  $PET$  function consisting of these coefficients mentioned in Table 6 was utilized to convert the downscaled  $T$  projections to  $PET$  values within the scope of RCP scenarios. Additionally, the parameters of the Ham-based simulation method with calibration and verification performances for each station are presented in Table 7.

According to the calculations made for the scenario period, there is no region in the Gediz Basin where the mean annual and seasonal  $PET$  are expected to decrease. On the monthly basis,  $PET$  decreases are generally expected only in January, February, and March in the major part of the basin. The minimum mean annual increases are foreseen in the Sarigol region as 4.2% for both RCP4.5 and RCP6.0 and 5.6% for RCP8.5, while the maximum increases are expected in the Demirci region, where relatively low  $PET$  was estimated in REF, as 7.4 and 10.2% for the related mid- and high-stabilization scenarios, respectively. When the  $PET$  column of Figure 6 is evaluated, it can be seen that the minimum  $PET$  increases may occur in the southern and western parts of the basin (Sarigol, Alasehir, Foca regions, and apart from these Simav region in the north). Moreover, the related increasing rate is foreseen to be exacerbated northeastwardly. The maximum increases are expected in the northern parts of the basin (Demirci and Gediz regions). As is the case with  $T$  projections, the  $PET$  changes were evaluated in terms of time periods for the entire basin. The mean total annual  $PET$ , which is 1,141.8 mm in REF, is expected to increase 5.5, 5.6, and 7.7% for RCP4.5, RCP6.0, and RCP8.5, respectively. For the seasonal periods, the mean total  $PET$  in an autumn season whose REF value is 219 mm is expected to have a maximum increase as 11.7, 12.1, and 15.2% for RCP4.5, RCP6.0, and RCP8.5, respectively. The increase rate of 5.6% in the winter and summer seasons and 0.81% in the spring season for RCP4.5, the increase rate of 6.8, 1, 5.4%, and 9, 2.6, 7.2% for RCP6.0 and RCP8.5 scenarios of winter, spring, and summer seasons, respectively, are foreseen in the scenario period. The maximum increase rate of  $PET$  is expected to occur in November for all of RCPs as in between 25 and 31% (see Figure 5). In order to analyze whether the possible  $PET$  changes are statistically significant, two sample  $t$ -tests were applied (the significance level is 0.05) as tested in the phase of  $T$  simulation. According to the  $t$ -tests, possible annual changes for all RCPs are statistically significant. The changes in the winter, summer, and autumn seasons are expected to be as statistically significant for all RCPs but only in the spring season is  $PET$  foreseen not to deviate significantly throughout the basin. The statistically significant changes are expected for

**Table 6** | The statistical performances of modified temperature-based *PET* methods

Station	Methods								
	Hamon			Thornthwaite			Blaney-Cridde		
	R <sup>2</sup>	NS	RSR	R <sup>2</sup>	NS	RSR	R <sup>2</sup>	NS	RSR
Akhisar	<u>0.979</u>	<u>0.979</u>	<u>0.144</u>	0.872	0.872	0.358	0.969	0.969	0.175
Alasehir	<u>0.985</u>	<u>0.985</u>	<u>0.121</u>	0.872	0.872	0.358	0.969	0.969	0.176
Demirci	<u>0.979</u>	<u>0.979</u>	<u>0.145</u>	0.869	0.869	0.361	0.966	0.965	0.187
Foca	<u>0.967</u>	<u>0.967</u>	<u>0.181</u>	0.879	0.879	0.347	0.956	0.956	0.209
Gediz	<u>0.980</u>	<u>0.980</u>	<u>0.142</u>	0.865	0.865	0.367	0.969	0.969	0.176
Golmamara	<u>0.979</u>	<u>0.979</u>	<u>0.143</u>	0.874	0.874	0.354	0.969	0.969	0.176
Gordes	<u>0.980</u>	<u>0.980</u>	<u>0.142</u>	0.896	0.896	0.322	0.964	0.963	0.191
Gure	<u>0.981</u>	<u>0.981</u>	<u>0.138</u>	0.876	0.876	0.351	0.969	0.969	0.176
Koprubasi	<u>0.983</u>	<u>0.983</u>	<u>0.132</u>	0.884	0.884	0.341	0.971	0.970	0.172
Kula	<u>0.986</u>	<u>0.986</u>	<u>0.116</u>	0.899	0.899	0.318	0.970	0.970	0.173
Manisa	<u>0.985</u>	<u>0.985</u>	<u>0.123</u>	0.880	0.880	0.346	0.971	0.971	0.171
Menemen	<u>0.975</u>	<u>0.975</u>	<u>0.158</u>	0.775	0.775	0.474	0.966	0.966	0.185
Salihli	<u>0.986</u>	<u>0.986</u>	<u>0.118</u>	0.859	0.859	0.376	0.970	0.970	0.173
Sarigol	<u>0.987</u>	<u>0.987</u>	<u>0.115</u>	0.865	0.865	0.367	0.970	0.970	0.174
Saruhanli	<u>0.978</u>	<u>0.978</u>	<u>0.148</u>	0.870	0.870	0.360	0.967	0.967	0.182
Selendi	<u>0.981</u>	<u>0.981</u>	<u>0.138</u>	0.888	0.888	0.334	0.968	0.967	0.181
Turguthu	<u>0.985</u>	<u>0.985</u>	<u>0.123</u>	0.883	0.883	0.342	0.969	0.969	0.176
Usak	<u>0.981</u>	<u>0.981</u>	<u>0.139</u>	0.899	0.899	0.318	0.969	0.968	0.178
Simav	<u>0.978</u>	<u>0.978</u>	<u>0.149</u>	0.882	0.882	0.343	0.964	0.964	0.190
Kemalpaşa	<u>0.984</u>	<u>0.984</u>	<u>0.127</u>	0.895	0.895	0.324	0.968	0.967	0.181

**Formulas:**

- $PET_{Ham} = a \left( \frac{D_L}{12} \right)^b e^{cT} + d$
- $PET_{Thw} = aK_t \left( \frac{bT_t}{J} \right)^k + c$
- $PET_{Bl-Cr} = kp(aT + b)$

**Case of Akhisar Station**

a: 114.252  
 b: 1.522  
 c: 0.021  
 d: -65.072

The coefficients a–d are calibrated in accordance with the PM method. The formulas given on the right are analogous with the original Ham, Bl–Cr, and Thw methods. The recalibrated coefficients of the Hamon formula and the scatter plot of Ham-based PM simulations are also given for the Akhisar meteorological station. The underlined values denote the best performances in each station.

the months between May and December in all RCPs, for April in the RCP8.5 scenario. It is not predicted that there will be any statistically significant changes for the rest of the months until 2050.

### 4.3. Future AI

In the study, the *PET* simulations for the 2015–2050 scenario period were derived for estimating future AI. As is known, UNEP AI is the function of mean annual *P* and mean annual *PET*. Prior to giving results about AI, we will briefly discuss the mean annual *P* simulations over the Gediz Basin from *OK16*. According to data utilized from *OK16*, it is predicted that 8.2, 10.2, and 17.2% decreases throughout the basin for RCP4.5, RCP6.0, and RCP8.5, respectively. A westward expansion of increasing absolute *P* decrease is foreseen and the absolute changes of possible decreases are maximum in the Menemen region for all RCPs. The sharpest decreases are expected in the mid-southern and western parts of the basin (Menemen, Foca, Koprubasi, Sarigol, and Salihli regions).

Due to the fact that it is expected in the future that there is no region where components of AI move towards humidity, the AI over the Gediz Basin is expected to tend to decrease in the scenario period. In REF, the DSH climate regime is observed in the eastern and northeastern parts of the basin. SA climate regime prevails in the major parts of the basin including central, western, and southern regions. The lowest long-term AI values of 0.35 are calculated for Sarigol and Alasehir regions and 0.36 for the Menemen region such that they are located in the southern and western parts of the basin, respectively. The SH climate regime is observed in Simav up northeast and in the Kemalpaşa region up southwest such that Simav has the highest long-term AI (0.81) in REF. The long-term AI is calculated as 0.46 for the entire basin which means the SA regime exists in the period 1980–2005. When examined region by region, 65% of the basin has the SA regime, 25% of the basin has the DSH regime and the SH regime is experienced in the rest of the basin. On a yearly basis, only in 4% of the time period 1980–2005, the AI gets the values between 0.65 and 1.0 which corresponds to SH climate characteristics, and in 38% of the time period, the AI gets the values between 0.5 and 0.65 corresponding to DSH climate characteristics. SA climate state arises in 58% of the time period such that it represents the main climatic characteristics of the basin for REF.

In the AI simulations, it is obtained that the AI is expected to decrease gradually with respect to REF for all regions of the basin as the radiative forcing increases. In other words, for all RCP scenarios, it is not foreseen that any H climate regime can be observed in the scenario period in any of the regions of the Gediz Basin. As in REF, in the western, central, and southern parts of the basin, the SA climate regime is foreseen to resume in the scenario period for all RCPs. In the RCP4.5 scenario, the

**Table 7** | The calibrated parameters of the Hamon-based simulation model and its performances

Station	Hamon parameters				Calibration			Verification		
	a	b	c	d	R <sup>2</sup>	NS	RSR	R <sup>2</sup>	NS	RSR
Akhisar	114.25	1.52	0.02	-65.07	0.980	0.980	0.142	0.979	0.978	0.147
Alasehir	157.58	1.37	0.01	-96.51	0.986	0.986	0.119	0.985	0.985	0.122
Demirci	103.72	1.54	0.02	-59.62	0.981	0.981	0.138	0.977	0.977	0.150
Foca	97.09	1.70	0.02	-41.21	0.970	0.969	0.175	0.966	0.965	0.186
Gediz	107.43	1.49	0.02	-59.56	0.983	0.982	0.132	0.978	0.978	0.150
Golmarmara	119.48	1.51	0.02	-69.10	0.981	0.980	0.140	0.979	0.979	0.145
Gordes	110.45	1.54	0.02	-63.70	0.983	0.982	0.134	0.978	0.978	0.148
Gure	112.48	1.50	0.02	-61.67	0.984	0.984	0.128	0.990	0.993	0.099
Koprubasi	122.43	1.47	0.02	-68.62	0.985	0.984	0.124	0.981	0.981	0.138
Kula	146.75	1.38	0.02	-95.27	0.987	0.986	0.116	0.987	0.987	0.116
Manisa	140.03	1.49	0.02	-85.69	0.986	0.985	0.122	0.985	0.985	0.123
Menemen	100.97	1.62	0.03	-57.13	0.973	0.973	0.164	0.977	0.977	0.152
Salihli	162.52	1.38	0.01	-100.56	0.988	0.987	0.112	0.985	0.985	0.123
Sangol	162.77	1.40	0.01	-100.36	0.988	0.988	0.111	0.986	0.986	0.118
Saruhanli	120.83	1.56	0.02	-68.77	0.980	0.979	0.145	0.978	0.977	0.150
Selendi	115.56	1.51	0.02	-67.88	0.981	0.981	0.139	0.981	0.981	0.137
Turgutlu	145.32	1.49	0.02	-89.66	0.986	0.985	0.122	0.985	0.985	0.123
Usak	115.41	1.44	0.02	-66.90	0.983	0.983	0.130	0.979	0.979	0.146
Simav	109.42	1.55	0.02	-59.54	0.981	0.981	0.138	0.975	0.975	0.158
Kemalpasa	131.79	1.57	0.02	-78.24	0.985	0.984	0.126	0.984	0.984	0.128

DSH climate regime is expected to prevail in the eastern and northeastern parts of the basin and the SH climate regime is expected to occur in Simav and Kemalpasa regions but with lower AI values. As experienced in the past period, the Simav region is foreseen to be the most humid region in the future for all RCPs (with AIs of 0.71, 0.69, 0.63 for RCP4.5, RCP6.0, and RCP8.5, respectively). In the RCP6.0 scenario, the climate regimes have the analogous spread as in the RCP4.5 but under drier climatic conditions than those of the REF and RCP4.5 scenario. In RCP8.5, it is expected that dryness may have more impact on the basin and there may be no region where the SH climate regime prevails. The results of the RCP8.5 scenario reveal that the most humid regions of the basin, Simav, and Kemalpasa, may have DSH climatic conditions in the future long-term. In addition to Simav and Kemalpasa, the Demirci region is expected to experience a DSH climate regime and SA climate conditions are expected to dominate in the rest of the basin. On the regional basis, 10% of the basin has the SH climate regime for both RCP4.5 and RCP6.0 scenarios as in REF, and it is not expected to be seen in any region of the basin in RCP8.5. The DSH climate regime is foreseen to occur in regions representing 10 and 15% of the basin in mid- and high-stabilization scenarios, respectively. Furthermore, the SA climate regime is expected to dominate over the basin with a rate of 80% for both RCP4.5 and RCP6.0 scenarios and 85% for RCP8.5. The long-term AI for the entire Gediz Basin is calculated as 0.40, 0.39, and 0.35 which are pronounced as SA climate regimes for all RCPs, and SA conditions are expected to be dominant over the entire basin in the future (Figure 6). On a yearly basis, the SH climate state is not expected to occur throughout the scenario period, the DSH climate state may occur in the 17, 22, and 6%, and the SA climate state may occur in the 83, 75, and 92% of the scenario period for RCP4.5, RCP6.0, and RCP8.5 scenarios, respectively. In addition, climatic states which correspond to AI values lower than 0.2 can possibly occur throughout the scenario period with the rate of 3%.

The annual temporal evolution of the direct and indirect components of AI itself was demonstrated in Figure 7. Moreover, Mann-Kendall trend tests with a 0.05 significance level were performed in order to investigate if there were statistically significant trends in each variable. As seen in the related figure, in REF and scenario projections there was almost no significant

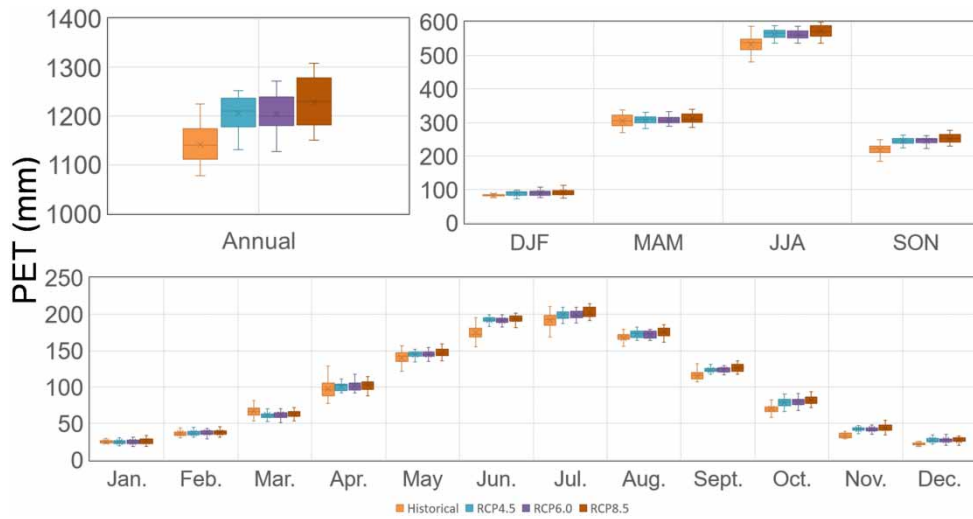


**Figure 5** | Box-plots of mean total annual, seasonal, and monthly *PET* projected under historical, RCP4.5, RCP6.0, and RCP8.5 scenarios. The acronyms labeled in the seasonal box-plots are same as in Figure 4.

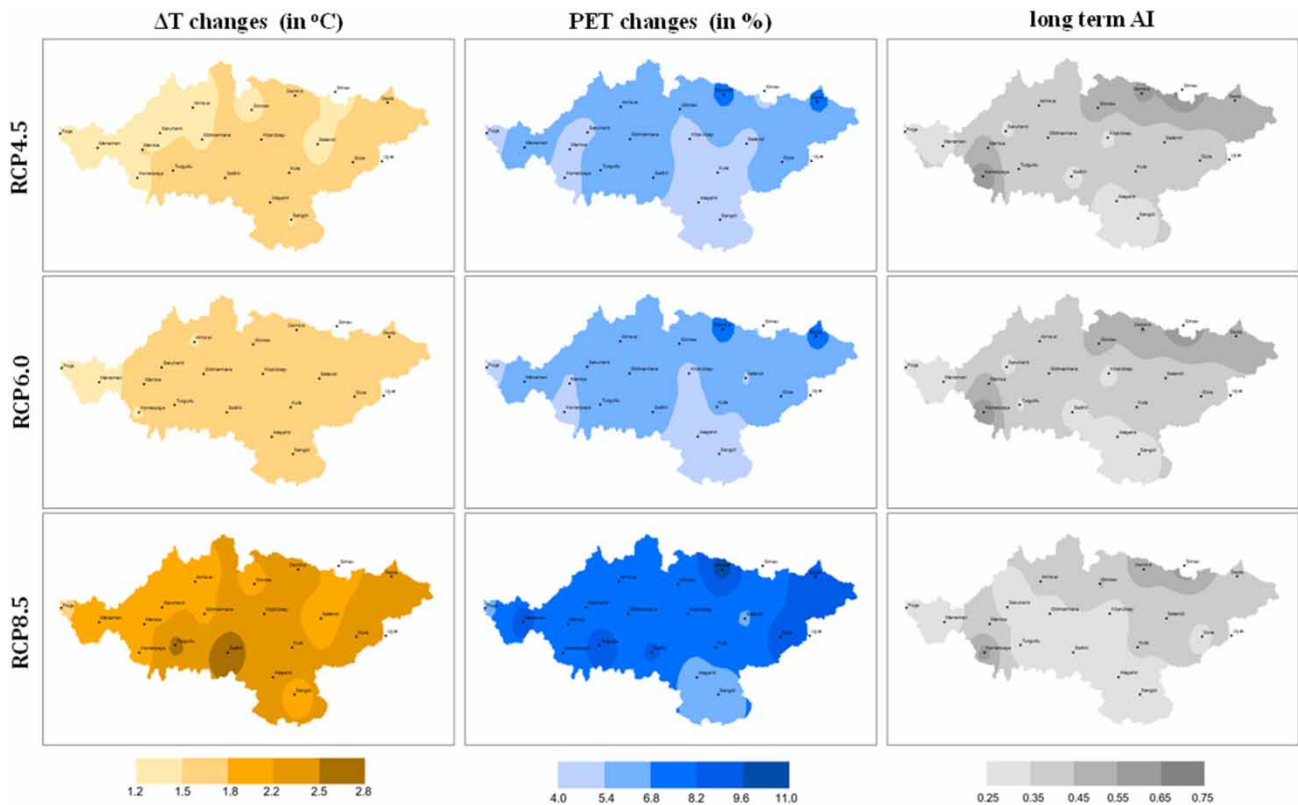


**Figure 6** | Spatial variability of mean annual *T* and *PET* and long-term AI over the Gediz Basin. ‘ $\Delta T$  Changes’ below the *T* column are equal to  $T_{RCP} - T_{Historical}$  and ‘% Changes’ below the *PET* column are equal to  $(PET_{RCP} - PET_{Historical})/PET_{Historical}$ .

trend in the *P* time series, however, for only the RCP6.0 scenario, a decreasing trend was estimated for *P*. As expected, for both *T* and *PET*, significant increasing trends were encountered with trend tests for REF and RCP scenarios. As for AI, a significant trend for REF and RCP4.5 was not predicted, however, a monotonic decreasing trend was seen in both RCP6.0 and



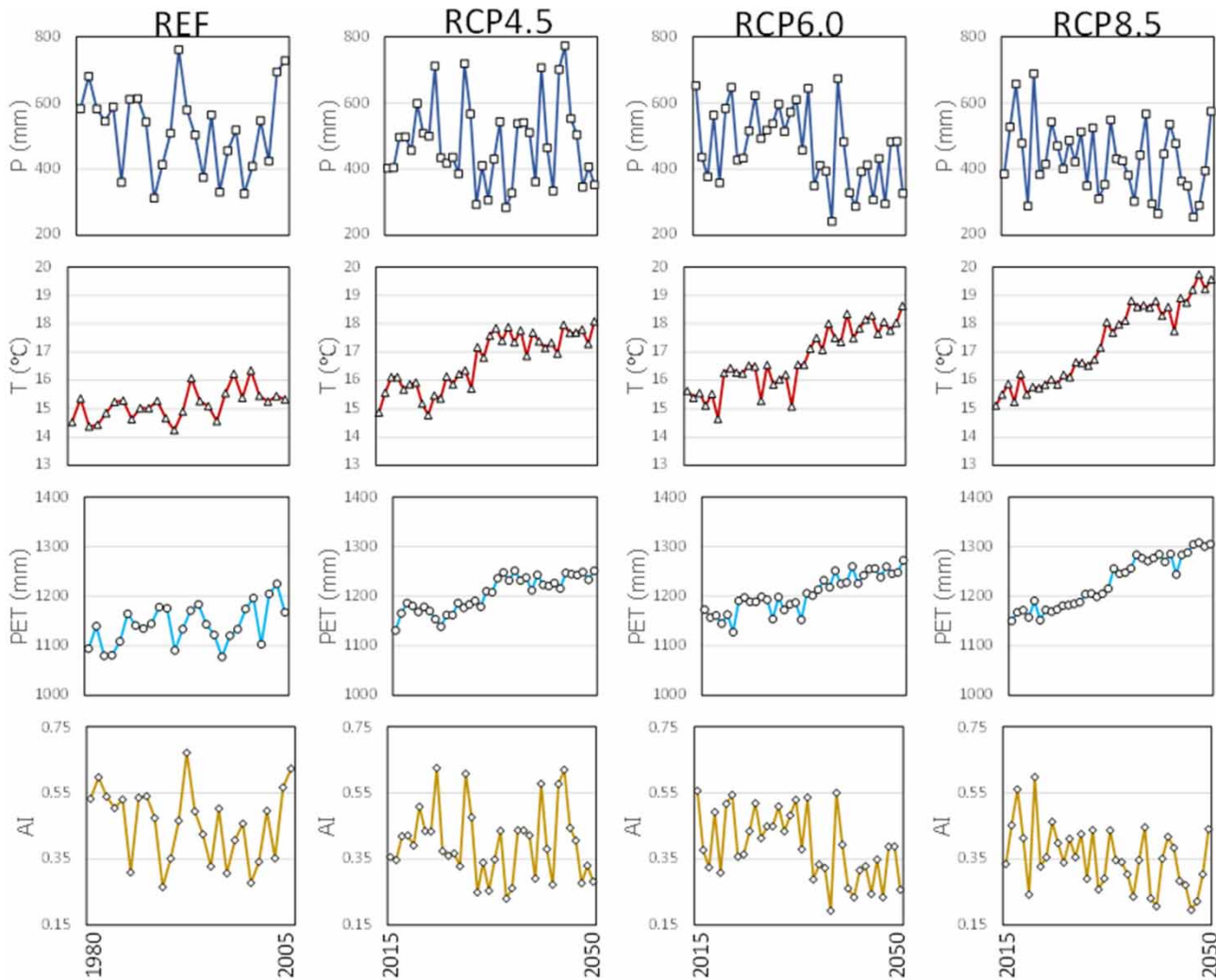


**Figure 7** | The temporal evolution of  $P$  (mm),  $T$  ( $^{\circ}\text{C}$ ),  $PET$  (mm), and  $AI$  for REF and RCP scenarios in the Gediz Basin. The columns from top to bottom represent the variables  $P$ ,  $T$ ,  $PET$ , and  $AI$ , respectively.

RCP8.5 scenarios. In conclusion, it can be interpreted that with the boosting of radiative forcing, the severe aridity is expected to increase in the basin such that the increment of  $T$  and  $PET$  are the prominent reasons.

## 5. DISCUSSION AND CONCLUSIONS

In this work, a projection algorithm was set up to analyze how  $AI$  over the Gediz Basin may change until the end of the mid-21st century. In order to do this implementation, a statistical downscaling procedure was applied so that coarse-resolution 12 GCMs data of three RCPs can be downscaled to the local scale. Following the downscaling stage, a multi-model ensemble and bias-correction strategy were applied through BMA and EDQM methods to achieve less uncertain, more robust, and unbiased  $T$  simulations. Ultimately, temperature projections with respect to three RCPs over the Gediz Basin were obtained. The  $T$ -based Ham, Bl-Cr, and Thw equations were modified with respect to  $PET$  estimates obtained through the PM method and hence, the data underlying the  $PET$  simulations were produced. The  $T$  simulations derived for three different RCPs were integrated with outperforming Ham-based  $PET$  equations and  $PET$  simulations that may occur over the Gediz Basin were obtained for the related concentration pathways. Subsequently, the  $AI$  and climatological regime which are expected over the Gediz Basin were predicted for the scenario period.

Statistical downscaling techniques are very useful methods to downscale raw GCM data to a local scale, especially in  $T$  downscaling. There are several studies made for different regions in the world in which statistical downscaling methods



derive very strong results for  $T$  downscaling (Chu *et al.* 2010; Jeong *et al.* 2012). In the study, ANN and LSSVM machine learning methods were employed to downscale  $T$  by utilizing the surface temperature variable of ERA-Interim reanalysis data as input. They both showed results classified as 'very good' for all meteorological stations, in fact, they have very high values of  $R^2$  as 0.98–0.99,  $NS$  as 0.98–0.99, and very low values of  $RSR$  as 0.08–0.12 for both calibration and verification stages of the models. What is more, the best downscaling results were derived by the models in terms of verification performances and the opportunity was constituted to utilize the results of both ANN and LSSVM. Hence, it is thought that these results are very consistent with the temperature simulations prepared for the study area.

Individual GCMs have uncertainty originating from different aspects such as initial and boundary condition uncertainties, problems in the theoretical definition of the global climate system, and parameter uncertainties (Knutti 2008). In the work, 12 GCMs were utilized instead of employing individual climate models in order to capture the varying notions of research centers that developed the related climate models. However, it is tedious to decide which climate models should be selected for the study area. In order to clear up this problem, the multi-GCM strategy developed for the study area was considered to be the key solution through the BMA model which assigns probabilistic weight for each GCM so that one deterministic result was obtained for each RCP. Moreover, by means of weight assignment, the BMA model gave us some idea about which climate model can be more predictive for the Gediz Basin with respect to different periods such as wet and dry. With this approach, BCC-CSM1.1 and HADGEM2-ES climate models can be thought as stochastically better explanatory models in comparison to the other ones for wet and dry periods, respectively.

The GCMs have inherent biases with respect to  $P$  and  $T$  such that they exist more in the predictions made for  $P$  due to the fact that the behaviour of  $P$  is more complex in comparison to that of temperature. In *OK16*, the  $P$  biases were corrected through the QM method where frequencies of model predictions are assigned with respect to distribution parameters of REF simulation and mapped onto the observed ones. The QM method is appropriate to utilize in  $P$  simulations, however, it may overestimate monthly temperature in so far as the future temperature is expected to exceed the historical range and the distribution does not change for the future adjustments. Hence, EDQM in which simulation distribution is taken into consideration was utilized in the study, and physically conceivable  $T$  simulations were derived.

Although PM is introduced as a reference method in the literature, its usage is sometimes troublesome on account of the lack of continuously observed data required by PM. Thus, an efficient strategy was implemented in the study by converting T-based methods in accordance with PM estimates. It enabled us to project  $PET$  by locally calibrated methods built upon down scalable  $T$  variables which were compatible with the mechanism of PM. Among the T-based methods, the Hamon method shows the best performance in that it utilizes only the duration of the daylight component in addition to  $T$ .

It is expected that the Gediz Basin has an increasing trend of  $T$  and  $PET$  in the scenario period. The highest mean annual change is expected to take place in the western, central, and southern parts of the basin. As is known,  $T$  is an effective factor causing  $PET$ , hence, it is natural that maximum increases in  $PET$  are expected in western, central, and southern parts where the most important water resources of the Gediz Basin such as Demirkopru Dam, Marmara Lake, Gordes Dam, Avsar Dam, and Buldan Dam are existing. Moreover, the irrigated fields are extending from the southern part to the western part of the basin. When it is thought that the mean areal  $P$  over these parts is expected to decrease, it may be inevitable that the irrigation water requirements may increase in the future. There is another study by Ozkul (2009) prepared for the future climate of the Gediz Basin. Overall, in Ozkul (2009), the GCMs of B2 and A2 emission scenarios of TAR and AR4 are utilized. According to  $T$  simulations (using only four meteorological stations), 1.2 and 2 °C changes by 2050 are predicted in B2 and A2 scenarios, respectively. B2 and A2 scenarios have similarities with RCP4.5 and RCP6.0, so, when the related simulations are compared to those prepared for this study, there are +0.35 and –0.4 °C differences between this study and Ozkul (2009). Furthermore, when mean annual  $PET$  results were compared for Menemen and Manisa stations (only the results of two meteorological stations are available) increases of 16% for B2 and 17% for A2 are expected in the Menemen station, and a 15% increase is expected in the Manisa station for both B2 and A2 scenarios, respectively. In this work, changes of 6.2% and 6.5% in Menemen and 5.3% and 5.4% for Manisa are expected for RCP4.5 and RCP6.0 scenarios, respectively. Although the results of the related study support this study, the use of different methodology, up-to-date scenarios, and comprehensive examination of the basin with 20 meteorological stations add to this study's novelty. In addition to Ozkul (2009), this study captures analogous results with Tabari & Willems (2018a) in which they find that western Turkey (also covering the Gediz Basin) in particular may experience decreases in  $P$  greater than 20% at the end of the 21st century. Moreover, they foresee that number of dry days and longest dry spell expected in the future may increase in the region. What is more, as claimed in studies

of Zarghami *et al.* (2011) and Nastos *et al.* (2013) prepared for Azerbaijan, Iran, and Greece which are neighboring countries of Turkey, they predict drier climate conditions than those of the past period as expected in our study.

In the literature, some references are related to topics such as signal-to-noise (S/N) interpretation and uncertainty decomposition theory in climate change impact assessments (Hawkins & Sutton 2011; Tabari & Willems 2018b) in which the sources of climatic variability are discussed. In this study, the issues such as detection of uncertainty stemmed from climate models or GHG concentration scenarios were not covered; however, internal variability was simply tackled in this section in brief. The coefficient of variation (CV) which can be considered as reciprocal of the S/N ratio was calculated for REF and RCPs and the reasons for AI variability were queried. Asfaw *et al.* (2018) and Hare (2003) have expressed that a higher value of the CV is the indicator of larger variability. Instead of checking S/N ratios, inter-annual CV statistics for  $T$ ,  $P$ , and AI were examined. Since the study is on the subject of projected aridity, the extent to which the variability in the AI was affected by the variations in  $P$  and  $T$  is investigated. At this stage, the inter-annual CV values calculated for the AI were analyzed by means of scattering diagrams (not presented here) in response to that of  $P$  and  $T$ , respectively. The obtained results demonstrated that inter-annual variability in the AI is more directed by  $P$  variability. Although it is monitored that the increase in inter-annual variability of  $T$  has an inverse effect on AI's variability, the correlations between them are not statistically significant. The main reason for this is that the trend in annual average  $T$  indicates a significant increase during the existed period, while the inter-annual irregularities in the  $P$  point out both no-trending and the large CV. In our future works, we have in view to deal with the methodologies, which were effectively applied by Tabari & Willems (2018b), to decompose total uncertainty into uncertainty originating from various stages of climate change projections.

Another noticeable finding obtained in the study is that the results of RCP4.5 and RCP6.0 are very close to each other. As known,  $PET$  is the function of  $T$  and AI is that of  $P$  and  $PET$ . Hence, it was decided by the authors to check out how raw GCM data of  $P$  and  $T$  vary for RCP4.5 and RCP6.0 scenarios. When examining the raw data of 12 GCM data, the similar close values draw attention to the scenario period. Overall, approximately the difference of  $-18$  mm which corresponds to 0.035% of the raw historical data in mean annual  $P$ , and of  $+0.1$  °C in mean annual  $T$  are projected by the climate models in the grids of study area. The range increases between the years 2051–2100 with the difference of  $-20$  mm (0.04% of raw historical data) and  $+0.4$  °C are projected in mean annual  $P$  and mean annual  $T$ , respectively. When the emission scenarios of AR5 are taken into consideration, the difference in GHG emission between the scenarios RCP4.5 and RCP6.0 are increasing right after the first half of the 21st century. Hence, it is logical to derive close results between RCP4.5 and RCP6.0 scenarios in the projections made for the first half of the 21st century. Moreover, there are other studies made in different regions of the world such as India (Chaturvedi *et al.* 2012) and North America (Swain & Hayhoe 2015) in which close results were derived for RCP4.5 and RCP6.0 scenarios.

Upon evaluating all simulations, it is obvious that negative effects of climate change on the Gediz Basin are expected in terms of aridity. In the past, the Gediz Basin experienced three types of climate regimes as SH, DSH, and SA in various regions of the area. The reason for possible negative effects of future climate on humid regions is that these regions are expected to have drier spells and conversion of the climate regime into DSH and SA in the Gediz Basin until the end of the mid-21st century. In terms of long-term AI, the climate regime in the REF is SA and this situation is not expected to change according to all of the RCPs. However, the values of AI which are calculated with respect to increasing GHG emission scenarios signify climate states forcing the A climate zone may come into existence in the conditions of RCPs. In the pessimistic scenario, it seems that the SA climate regime may overwhelmingly dominate the study area. When assessed on a regional basis, the driest parts of the region may exist in the lower Gediz Basin where Avsar and Buldan irrigation dams are operated for the agricultural fields. Moreover, the central and western parts of the basin where the other water resources exist are in the tendency of being in the SA climate zone. Bannayan *et al.* (2010) made a study about the correlation between agricultural productivity and AIs in Iran and found a positive correlation between grain yield and AI. Hence, due to the fact that agricultural activities are intensely available in the Gediz Basin, it is recommended by the authors that a study should be made about how agricultural productivity may change in the future with respect to aridity for the sustainability of the agricultural sector.

## DATA AVAILABILITY STATEMENT

Data cannot be made publicly available; readers should contact the corresponding author for details.

## CONFLICT OF INTEREST

The authors declare there is no conflict.

## REFERENCES

- Anandhi, A., Srinivas, V. V., Nanjundiah, R. S. & Kumar, D. N. 2008 Downscaling precipitation to river basin in India for IPCC SRES scenarios using support vector machine. *International Journal of Climatology* **28** (3), 401–420.
- Asfaw, A., Simane, B., Hassen, A. & Bantider, A. 2018 Variability and time series trend analysis of rainfall and temperature in northcentral Ethiopia: a case study in Woleka sub-basin. *Weather and Climate Extremes* **19**, 29–41. <https://doi.org/10.1016/j.wace.2017.12.002>.
- Bannayan, M., Sanjani, S., Alizadeh, A., Lotfabadi, S. S. & Mohamadian, A. 2010 Association between climate indices, aridity index, and rainfed crop yield in northeast of Iran. *Field Crops Research* **118** (2), 105–114. <https://doi.org/10.1016/j.fcr.2010.04.011>.
- Budyko, M. I. 1958 *The Heat Balance of the Earth's Surface*. Dept. of Commerce, Weather Bureau, Washington, DC.
- Chaturvedi, R. K., Joshi, J., Jayaraman, M., Bala, G. & Ravindranath, N. H. 2012 Multi-model climate change projections for India under representative concentration pathways. *Current Science* **103** (7), 791–802.
- Chen, J., Brissette, F. P., Lucas-Picher, P. & Caya, D. 2017 Impacts of weighting climate models for hydro-meteorological climate change studies. *Journal of Hydrology* **549** (October), 534–546. <https://doi.org/10.1016/j.jhydrol.2017.04.025>.
- Chu, J. T., Xia, J., Xu, C. Y. & Singh, V. P. 2010 Statistical downscaling of daily mean temperature, pan evaporation and precipitation for climate change scenarios in Haihe River, China. *Theoretical and Applied Climatology* **99** (1–2), 149–161. <https://doi.org/10.1007/s00704-009-0129-6>.
- Dascălu, S. I., Gothard, M., Bojariu, R., Birsan, M. V., Cică, R., Vintila, R., Adler, M. J., Chendeş, V. & Mic, R. P. 2016 Drought-related variables over the Bârlad basin (Eastern Romania) under climate change scenarios. *Catena* **141**, 92–99. <https://doi.org/10.1016/j.catena.2016.02.018>.
- Dibike, Y. B., Gachon, P., St-Hilaire, A., Ouarda, T. B. M. J. & Nguyen, V. T. V. 2007 Uncertainty analysis of statistically downscaled temperature and precipitation regimes in Northern Canada. *Theoretical and Applied Climatology* **91** (1–4), 149–170. <https://doi.org/10.1007/s00704-007-0299-z>.
- Fernandez, J. P. R., Franchito, S. H., Rao, V. B. & Llopart, M. 2017 Changes in Koppen–Trewartha climate classification over South America from RegCM4 projections. *Atmospheric Science Letters* **18** (11), 427–434. <https://doi.org/10.1002/asl.785>.
- Fistikoglu, O. & Okkan, U. 2011 Statistical downscaling of monthly precipitation using NCEP/NCAR reanalysis data for Tahtali river basin in Turkey. *Journal of Hydrologic Engineering* **16** (2), 157–164. [https://doi.org/10.1061/\(ASCE\)HE.1943-5584.0000300](https://doi.org/10.1061/(ASCE)HE.1943-5584.0000300).
- Hare, W. 2003 Assessment of knowledge on impacts of climate change – contribution to the specification of the Art.2 of the UNFCCC. In: *Wissenschaftlicher Beirat der Bundesregierung Globale Umweltveränderungen*, Potsdam, Berlin.
- Hawkins, E. & Sutton, R. 2011 The potential to narrow uncertainty in projections of regional precipitation change. *Climate Dynamics* **37** (1), 407–418. <https://doi.org/10.1007/s00382-010-0810-6>.
- IPCC 2010 *Meeting Report of the Intergovernmental Panel on Climate Change Expert Meeting on Assessing and Combining Multi Model Climate Projections* (Stocker, T. F., Qin, D., Plattner, G.-K., Tignor, M. & Midgley, P. M., eds.). IPCC Working Group I Technical Support Unit, University of Bern, Bern, Switzerland.
- IPCC 2013 *Climate Change 2013 - The Physical Science Basis*. Contribution of Working Group I to the Fifth Assessment Report of the Intergovernmental Panel on Climate Change, 1535.
- Jeong, D. I., St-Hilaire, A., Ouarda, T. B. M. J. & Gachon, P. 2012 Comparison of transfer functions in statistical downscaling models for daily temperature and precipitation over Canada. *Stochastic Environmental Research and Risk Assessment* **26** (5), 633–653. <https://doi.org/10.1007/s00477-011-0523-3>.
- Knutti, R. 2008 Should we believe model predictions of future climate change? *Philosophical Transactions Series A, Mathematical, Physical, and Engineering Sciences* **366** (1885), 4647–4664. <https://doi.org/10.1098/rsta.2008.0169>.
- Krikken, F., Lehner, F., Hausteine, K., Drobyshev, I. & Oldenborgh, G. J. 2021 Attribution of the role of the climate change in the forest fires in Sweden 2018. *Natural Hazards and Earth System Sciences* **21**, 2169–2179.
- Kwon, W., Baek, H. & Park, E. 2010 Probabilistic regional climate change projections using Bayesian model averaging. In: *IPCC Expert Meeting on Assessing and Combining Multi Model Climate Projections*, Boulder, Colorado, USA.
- Le Roux, R., Katurji, M., Zawar-Reza, P., Quéno, H. & Sturman, A. 2018 Comparison of statistical and dynamical downscaling results from the WRF model. *Environmental Modelling and Software* **100** (December 2017), 67–73. <https://doi.org/10.1016/j.envsoft.2017.11.002>.
- Li, H., Sheffield, J. & Wood, E. F. 2010 Bias correction of monthly precipitation and temperature fields from Intergovernmental Panel on Climate Change AR4 models using equidistant quantile matching. *Journal of Geophysical Research Atmospheres* **115** (10). <https://doi.org/10.1029/2009JD012882>.
- Lin, L., Gettelman, A., Fu, Q. & Xu, Y. 2018 Simulated differences in 21st century aridity due to different scenarios of greenhouse gases and aerosols. *Climatic Change* **146** (3–4), 407–422. <https://doi.org/10.1007/s10584-016-1615-3>.
- Maliva, R. & Missimer, T. 2012 *Arid Lands Water Evaluation and Management*, Environmental Science and Engineering. Springer, Berlin, Heidelberg. [https://doi.org/10.1007/978-3-642-29104-3\\_2](https://doi.org/10.1007/978-3-642-29104-3_2).
- Marengo, J. A. & Bernasconi, M. 2015 Regional differences in aridity/drought conditions over Northeast Brazil: present state and future projections. *Climatic Change* **129** (1–2), 103–115. <https://doi.org/10.1007/s10584-014-1310-1>.



- Miao, C., Duan, Q., Sun, Q. & Li, J. 2013 Evaluation and application of Bayesian multi-model estimation in temperature simulations. *Progress in Physical Geography* **37** (6), 727–744. <https://doi.org/10.1177/0309133313494961>.
- Min, S. K., Simonis, D. & Hense, A. 2007 Probabilistic climate change predictions applying Bayesian model averaging. *Philosophical Transactions of the Royal Society A: Mathematical, Physical and Engineering Sciences* **365** (1857), 2103–2116. <https://doi.org/10.1098/rsta.2007.2070>.
- Moriasi, D. N., Arnold, J. G., Van Liew, M. W., Binger, R. L., Harmel, R. D. & Veith, T. L. 2007 Model evaluation guidelines for systematic quantification of accuracy in watershed simulations. *Transactions of the ASABE* **50** (3), 885–900. <https://doi.org/10.13031/2013.23153>.
- Murphy, M. J., Sexton, H. D., Barnett, N., Jones, S., Webb, J. & Collins, M. 2004 Quantification of modelling uncertainties in a large ensemble of climate change simulations. *Nature* **430** (7001), 768–772. <https://doi.org/10.1038/nature02770.1>.
- Nastos, P. T., Politi, N. & Kapsomenakis, J. 2013 Spatial and temporal variability of the Aridity Index in Greece. *Atmospheric Research* **119**, 140–152. <https://doi.org/10.1016/j.atmosres.2011.06.017>.
- Okkan, U. & Inan, G. 2015 Statistical downscaling of monthly reservoir inflows for Kemer watershed in Turkey: use of machine learning methods, multiple GCMs and emission scenarios. *International Journal of Climatology* **35** (11), 3274–3295. <https://doi.org/10.1002/joc.4206>.
- Okkan, U. & Kirdeemir, U. 2016 Downscaling of monthly precipitation using CMIP5 climate models operated under RCPs. *Meteorological Applications* **23** (3), 514–528. <https://doi.org/10.1002/met.1575>.
- Okkan, U. & Kiyamaz, H. 2019 Questioning of empirically derived and locally calibrated potential evapotranspiration equations for a lumped water balance model. *Journal of Water and Climate Change*. <https://doi.org/10.2166/wcc.2019.292>.
- Ozkul, S. 2009 Assessment of climate change effects in aegean river basins: the case of gediz and buyuk menderes basins. *Climatic Change* **97** (1), 253–283. <https://doi.org/10.1007/s10584-009-9589-z>.
- Paltineanu, C., Mihailescu, I. F., Seceleanu, I., Dragota, C. & Vasenciu, F. 2007 Using aridity indices to describe some climate and soil features in Eastern Europe: a Romanian case study. *Theoretical and Applied Climatology* **90** (3–4), 263–274. <https://doi.org/10.1007/s00704-007-0295-3>.
- Raftery, A. E., Gneiting, T., Balabdaoui, F. & Polakowski, M. 2005 Using Bayesian model averaging to calibrate forecast ensembles. *Monthly Weather Review* **133** (5), 1155–1174. <https://doi.org/10.1175/MWR2906.1>.
- Scheff, J. & Frierson, D. M. W. 2015 Terrestrial aridity and its response to greenhouse warming across CMIP5 climate models. *Journal of Climate* **28** (14), 5583–5600. <https://doi.org/10.1175/JCLI-D-14-00480.1>.
- Schoof, J. T. 2013 Statistical downscaling in climatology. *Geography Compass* **7** (4), 249–265. <https://doi.org/10.1111/gec3.12036>.
- Smakhtin, V. U. & Schipper, E. L. F. 2008 Droughts: the impact of semantics and perceptions. *Water Policy* **10** (2), 131–143. <https://doi.org/10.2166/wp.2008.036>.
- Smith, I. & Chandler, E. 2010 Refining rainfall projections for the Murray Darling Basin of south-east Australia—the effect of sampling model results based on performance. *Climatic Change* **102** (3), 377–393. <https://doi.org/10.1007/s10584-009-9757-1>.
- Swain, S. & Hayhoe, K. 2015 CMIP5 projected changes in spring and summer drought and wet conditions over North America. *Climate Dynamics* **44**, 2737–2750. [https://doi.org/10.1061/\(asce\)he.1943-5584.0000366](https://doi.org/10.1061/(asce)he.1943-5584.0000366).
- Tabari, H. & Talaei, P. H. 2011 Local calibration of the hargreaves and priestley-taylor equations for estimating reference evapotranspiration in arid and cold climates of Iran based on the Penman-Monteith Model. *Journal of Hydrologic Engineering* **16** (10), 837–845. [https://doi.org/10.1061/\(asce\)he.1943-5584.0000366](https://doi.org/10.1061/(asce)he.1943-5584.0000366).
- Tabari, H. & Willems, P. 2018a More prolonged droughts by the end of the century in the Middle East. *Environmental Research Letters* **13** (10). <https://doi.org/10.1088/1748-9326/aae09c>.
- Tabari, H. & Willems, P. 2018b Seasonally varying footprint of climate change on precipitation in the Middle East. *Scientific Reports* **8** (1), 2–11. <https://doi.org/10.1038/s41598-018-22795-8>.
- Tuel, A., Kang, S. & Eltahir, E. A. B. 2020 Understanding climate change over the southwestern Mediterranean using high-resolution simulations. *Climate Dynamics* **56**, 985–1001. <https://doi.org/10.1007/s00382-020-05516-8>.
- UNEP 1992 *World Atlas of Desertification*. Edward Arnold, London.
- UNESCO 1979 *Map of the World Distribution of Arid Regions*. Explanatory Note UNESCO, Paris.
- Wang, B., Zheng, L., Liu, D. L., Ji, F., Clark, A. & Yu, Q. 2018 Using multi-model ensembles of CMIP5 global climate models to reproduce observed monthly rainfall and temperature with machine learning methods in Australia. *International Journal of Climatology* **38**, 4891–4902.
- Whetton, P., Macadam, I., Bathols, J. & O'Grady, J. 2007 Assessment of the use of current climate patterns to evaluate regional enhanced greenhouse response patterns of climate models. *Geophysical Research Letters* **34** (14), 1–5. <https://doi.org/10.1029/2007GL030025>.
- Xu, C. & Singh, V. P. 2001 Evaluation and generalization of temperature-based methods for calculating evaporation. *Hydrological Processes* **15** (2), 305–319.
- Yang, T., Hao, X., Shao, Q., Xu, C. Y., Zhao, C., Chen, X. & Wang, W. 2012 Multi-model ensemble projections in temperature and precipitation extremes of the Tibetan Plateau in the 21st century. *Global and Planetary Change* **80–81**, 1–13. <https://doi.org/10.1016/j.gloplacha.2011.08.006>.
- Yin, Y., Ma, D., Wu, S. & Pan, T. 2015 Projections of aridity and its regional variability over China in the mid-21st century. *International Journal of Climatology* **35** (14), 4387–4398. <https://doi.org/10.1002/joc.4295>.
- Zarghami, M., Abdi, A., Babaeian, I., Hassanzadeh, Y. & Kanani, R. 2011 Impacts of climate change on runoffs in East Azerbaijan, Iran. *Global and Planetary Change* **78** (3–4), 137–146. <https://doi.org/10.1016/j.gloplacha.2011.06.003>.